SSD-TDR-63-78

REPORT NO.
TDR-169(3230-12)TR-3

Shock Tube Test Time Limitation Due to Turbulent Wall Boundary Layer

6 MAY 1963

Prepared by HAROLD MIRELS
Aerodynamics and Propulsion Research Laboratory

Prepared for COMMANDER SPACE SYSTEMS DIVISION
UNITED STATES AIR FORCE
Inglewood, California

LABORATORIES DIVISION • AEROSPACE CORPORATION
CONTRACT NO. AF 04(695)-169

SSD-TDR-63-78

Report No.
TDR-169(3230-12)TR-3

SHOCK TUBE TEST TIME LIMITATION DUE TO TURBULENT WALL BOUNDARY LAYER

Prepared by

Harold Mirels
Aerodynamics and Propulsion Research Laboratory

AEROSPACE CORPORATION
El Segundo, California

Contract No. AF 04(695)-169

6 May 1963

Prepared for

COMMANDER SPACE SYSTEMS DIVISION
UNITED STATES AIR FORCE
Inglewood, California

ABSTRACT

Shock tube test time limitation due to the premature arrival of the contact surface is analytically investigated for wholly turbulent wall boundary layers. The results are compared with those for wholly laminar wall boundary layers. It is found that for a given shock Mach number, M_s, the maximum possible test time (in a long shock tube) varies as $d^{5/4}p_\infty^{1/4}$ and d^2p_∞ for the turbulent and laminar cases, respectively (d = tube diam, p_∞ = initial pressure). For $3 \leq M_s \leq 8$ in air or argon, it is found that the turbulent boundary layer theory for maximum test time applies for $dp_\infty \gtrsim 4$ to 10 (air) and $dp_\infty \gtrsim 2$ to 10 (argon), where d is in inches, p_∞ is in cm Hg. Similarly, for $3 \leq M_s \leq 8$, the laminar theory applies for $dp_\infty \lesssim 0.3$ (air) and $dp_\infty \lesssim 0.6$ to 1 (argon). When $dp_\infty \approx 5$, turbulent theory for both air and argon indicates test times of about 1/2 to 1/4 the ideal value for $x_s/d = 45$ to 150, respectively (x_s = length of low pressure section). Higher values of dp_∞ result in more test time. When $dp_\infty \approx 0.5$, laminar theory indicates about 1/2 ideal test time for $x_s/d \approx 100$. Lower dp_∞ reduces test time. Working curves are presented for more accurate estimates of test time in specific cases.

CONTENTS

FIGURES

TABLES

I. INTRODUCTION

In an ideal inviscid shock tube, the separation distance between shock and contact surface increases linearly with distance from the diaphragm (Fig. 1). In a real shock tube, however, the wall boundary layer between the shock and contact surface acts as an aerodynamic sink and absorbs mass from this region. This causes the contact surface to accelerate and the shock to decelerate and reduces the separation distance, ℓ, below the ideal value. The separation distance approaches a limiting (maximum) value, ℓ_m. At this limiting condition, the shock and contact surface both move with the same velocity (Fig. 1). The limiting separation distance is that at which the mass flow entering the shock equals the boundary layer mass flow moving past the contact surface.

Separation distance imposes an upper bound on the test time in shock tubes. (Nonuniformity of the flow between shock and contact surface may further reduce test time. The amount of flow nonuniformity that can be tolerated depends on the nature of the experiment and the instrumentation.) It is thus important to know separation distance as a function of distance from the diaphragm in order to estimate test times in shock tubes.

The effect of a laminar wall boundary layer on separation distance has been studied experimentally by Duff (Ref. 1) and both experimentally and analytically by Roshko (Ref. 2) and Hooker (Ref. 3). Some aspects of the analyses presented in Refs. 2 and 3 are modified in Ref. 4. These references can be used to estimate test time in low pressure shock tubes (roughly, those shock tubes with initial pressures of the order of 1 mm Hg or less, currently being used to study dissociation, ionization, and other rate phenomena). The test time limitation in low pressure shock tubes has received considerable attention because the upper limit on test time is proportional to $d^2 p_\infty$ (Ref. 2) and very low $d^2 p_\infty$ can result in virtually no usable test time (d = tube diam, p_∞ = initial pressure).

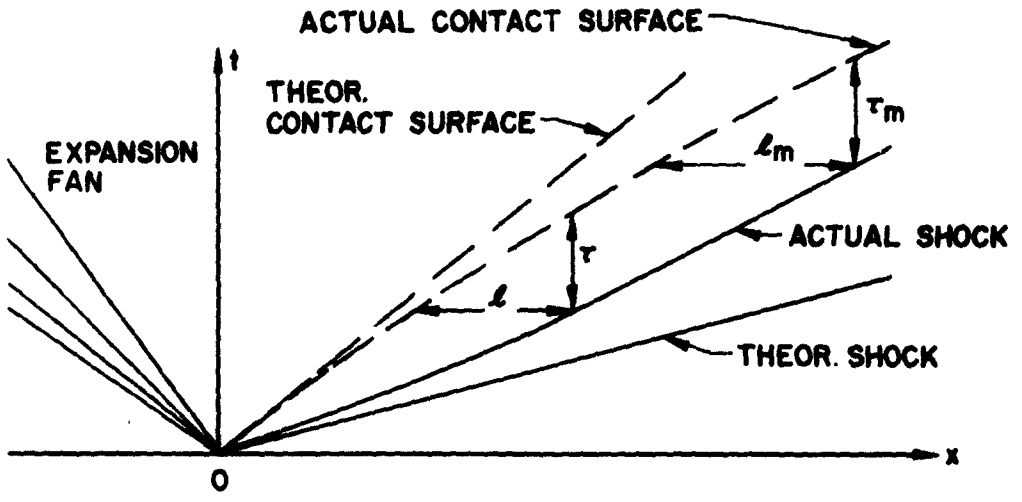

(a) t-x Diagram

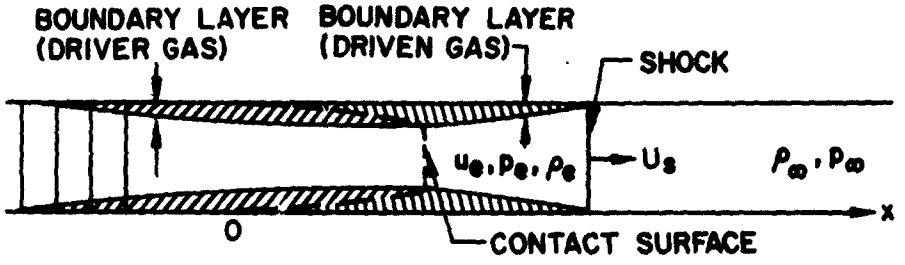

(b) Laboratory Flow

Fig. 1. Boundary Layer Effect on Shock Tube Flow

The effect of a turbulent wall boundary layer on separation distance has been treated only by Anderson (Ref. 5). It is interesting to note that Anderson was the first to blame less than ideal shock tube test time on the premature arrival of the contact surface. Anderson showed, for two practical examples, that mass loss to a turbulent wall boundary layer reduced the theoretical test time by about a half. This was in agreement with a rule-of-thumb presented in Ref. 6 for shock tubes used to study re-entry heat transfer. In Ref. 6, it was stated that 40 to 70 percent of theoretical test time was generally obtained, and 50 percent was proposed as a mean value. (The test time referred to was the period of essentially uniform conditions. The reduction from the ideal value was attributed, in Ref. 6, to mixing at the interface and flow nonuniformity associated with shock attenuation rather than to the premature arrival of the contact surface). Since test time did not appear to represent a serious problem in re-entry heat transfer shock tubes studies, the work of Anderson did not find widespread application.

As previously noted, the effect of a laminar boundary layer on shock tube test time is now receiving considerable attention (Refs. 1-4). It is therefore felt that it is worthwhile to develop the turbulent boundary layer case beyond the preliminary work of Anderson. Anderson presented a first estimate of the variation of separation distance with distance from the diaphragm for a particular initial pressure (10 cm Hg) and two tube diameters (1-1/2 and 4 in.). In the present paper, the problem is formulated more accurately, and the results are presented in nondimensional form so as to be applicable for arbitrary initial pressures and tube diameters. Criteria are established to define when turbulent wall boundary layer theory is applicable and when laminar wall boundary layer theory is applicable. The development here is parallel to that used in Ref. 4 for the laminar case.

The present solution is primarily intended for the case where the wall boundary layer introduces sizable reductions in test time. When the wall boundary layer introduces only small perturbations of the ideal test time, the linearized methods of Refs. 15 and 16 are more appropriate.

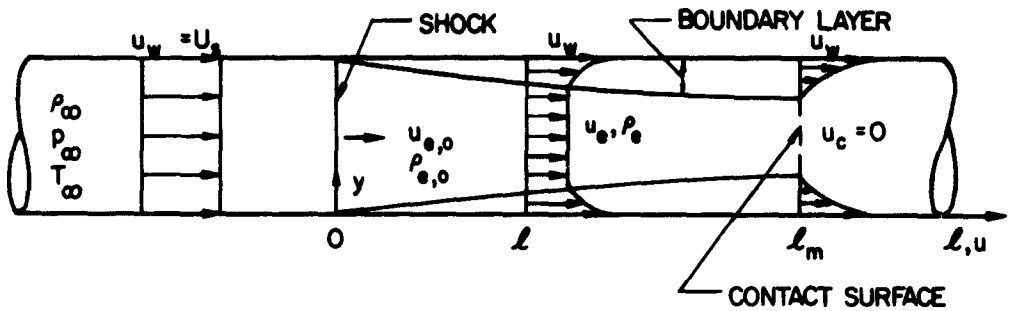

(a) Nonuniform Free Stream

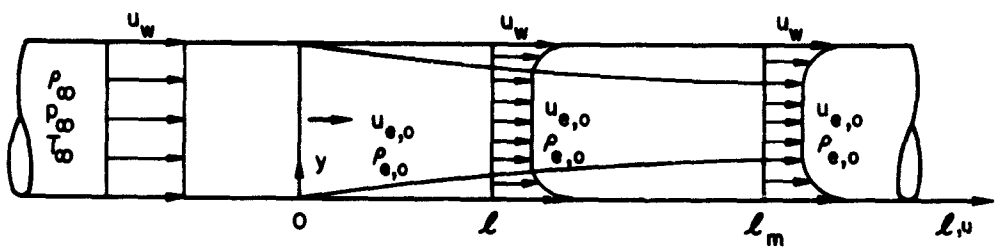

(b) Uniform Free Stream

Fig. 2. Flow Between Shock and Contact Surface in Shock-Stationary Coordinate System

II. MAXIMUM SEPARATION DISTANCE

Due to the wall boundary layer, the separation distance between shock and contact surface approaches a maximum value such that the mass flow through the shock equals the mass flow moving past the contact surface. This phenomenon has been observed for laminar wall boundary layers (Refs. 1-3) and may also be assumed to occur, for sufficiently long shock tubes, in the case of a turbulent wall boundary layer. When the maximum separation distance is reached, both shock and contact surface move with the same velocity.* The flow between the shock and contact surface may then be viewed as steady in a coordinate system in which the shock is stationary. In this shock-stationary coordinate system, the wall moves with velocity u_w (which equals the shock velocity U_s in the laboratory system). This steady flow is investigated in this section with the primary object of determining the maximum separation distance between the shock and the contact surface. The variation of separation distance with distance from the diaphragm is treated in Section III.

The steady flow is illustrated in Fig. 2a. The shock is located at $\ell = 0$, and the free stream portion of the contact surface at $\ell = \ell_m$. The flow upstream of the shock is denoted by subscript ∞ and moves with velocity u_w, as does the wall. Free stream conditions between the shock and the contact surface are denoted by subscript e. Free stream conditions directly downstream of the shock have the additional subscript o. The percentage of mass flow in the boundary layer increases with ℓ such that all the mass flow is in the boundary layer at ℓ_m, and the free stream is stationary at that location.

*For laminar boundary layers, the shock and contact surface velocities tend to remain constant after the maximum separation distance is reached (Ref. 1). For turbulent wall boundary layers, the shock and contact surface may both continue to decelerate after the maximum separation is reached. This deceleration depends on the driver gas. If the shock continues to decelerate, then the present steady solution is a quasi-steady solution.

The physical parameters upon which ℓ_m depends can be found as follows. The flow rate through the shock, $\dot{m}_s$, is

$$\dot{m}_s = (\rho_e u_e)_o A = \rho_\infty u_w A \tag{1a}$$

where A is the cross-sectional area of the tube. If it is assumed that the boundary layer is thin relative to the tube radius, the mass flow in the boundary layer at the contact surface location, $\dot{m}_c$, can be characterized by

$$\dot{m}_c = L\rho_{w,o}(u_w - u_{e,o})\delta_R \tag{1b}$$

where

$$\delta_R \equiv \beta \ell_m^{1-n}\left(\frac{\nu_{w,o}}{u_w - u_{e,o}}\right)^n \tag{1c}$$

Here, L is the perimeter of the tube; δ_R is a characteristic boundary layer displacement thickness at ℓ_m; $\rho_{w,o}$ and $u_w - u_{e,o}$ are characteristic densities and velocities, respectively; β is a constant; and n = 1/2 for laminar and 1/5 for turbulent boundary layers. Equating Eqs. (1a) and (1b) yields

$$\ell_m^{1-n} = \frac{d}{4\beta}\frac{\rho_{e,o}}{\rho_{w,o}}\frac{u_{e,o}}{u_w - u_{e,o}}\left(\frac{u_w - u_{e,o}}{\nu_{w,o}}\right)^n \tag{2}$$

where d = 4A/L is the hydraulic diameter of the tube.

Assume that the temperature upstream of the shock is at a standard condition so that $T_\infty = T_{st}$, $a_\infty = a_{st}$, and $\mu_\infty = \mu_{st}$. Also, assume that the

wall remains at its initial temperature so that $T_w = T_{st}$. Equation (2) can now be put in the form

$$\left(\frac{p_{st}}{p_\infty}\right)^n \frac{\ell_m^{1-n}}{d} = \frac{1}{4\beta}\left(\frac{p_\infty}{p_{e,o}}\frac{W}{W-1}\right)^{1-n} M_s^n \left(\frac{\rho a}{\mu}\right)_{st}^n \tag{3}$$

where $W = u_w/u_{e,o} = \rho_{e,o}/\rho_\infty$; $M_s = u_w/a_\infty$; and p_{st} is a standard pressure, usually taken to be one atmosphere. For $n = 1/2$, these equations reduce to those presented in Ref. 4. For $n = 1/5$, Eq. (3) becomes

$$\left(\frac{p_{st}}{p_\infty}\right)^{1/4} \frac{\ell_m}{d^{5/4}} = \left(\frac{1}{4\beta}\right)^{5/4} \frac{p_\infty}{p_{e,o}} \frac{W}{W-1} M_s^{1/4} \left(\frac{\rho a}{\mu}\right)_{st}^{1/4} \tag{4}$$

The right-hand side of Eq. (3) depends primarily on M_s. For a given M_s, $\ell_m \sim d^2 p_\infty$ for a laminar boundary layer, and $\ell_m \sim d^{5/4} p_\infty^{1/4}$ for a turbulent boundary layer. Therefore, for turbulent boundary layers, ℓ_m is less sensitive to variations of d and p_∞ than is the case for laminar boundary layers.

Equation (4) does not yield numerical results for ℓ_m unless an accurate estimate of β is available. Actually, β must be found from ℓ_m, rather than vice versa. That is, Eq. (2) is taken as defining β, that is,

$$\beta \equiv \frac{d}{4\ell_m^{1-n}} \frac{p_\infty}{p_{e,o}} \frac{W}{W-1}\left(\frac{u_w - u_{e,o}}{\nu_{w,o}}\right)^n \tag{5}$$

and ℓ_m is found as accurately as possible from a consideration of the boundary layer development in Fig. 2a. A first estimate for β, termed β_o, is made below by assuming the boundary layer to develop in a uniform external stream. An improved estimate, termed β_1, is then made by

considering a variable external stream and employing the concept of local boundary layer similarity.

A. UNIFORM EXTERNAL FREE STREAM APPROXIMATION

Boundary layer development for the case of an external free stream that does not vary with ℓ is illustrated in Fig. 2b and is discussed in Appendix A. Let ℓ_m correspond to the value of ℓ at which the excess mass flow in the boundary layer equals the mass flow entering through the shock. The mass flow past the contact surface is then

$$\frac{\dot{m}_c}{L(\rho_e u_e)_o} = -\delta^*_m \cong K_o \ell_m^{4/5} \left(\frac{\nu_{w,o}}{u_w - u_{e,o}} \right)^{1/5} \tag{6}$$

where δ^*_m is the displacement thickness at ℓ_m and K_o is a function defined in Appendix A. Equating Eqs. (1b), (1c), and (6) then yields

$$\beta_o = \frac{p_\infty}{p_{e,o}} \frac{W}{W-1} K_o \tag{7}$$

Values of β_o have been computed for $\gamma = 7/5$, $\sigma = 0.72$ and $\gamma = 5/3$, $\sigma = 0.67$ using the turbulent boundary layer theory of Appendix A together with the Sutherland viscosity law. (γ = ratio of specific heats, σ = Prandtl number). Values of β_o have also been computed for the flow behind strong shocks in air at initial pressures of 0.5 and 10 cm Hg. These four cases are further identified in Table 1 and the numerical results for β_o are listed in Table 2. These values of β_o can be used to find turbulent boundary layer displacement thickness (Eqs. 6, 7) and will be used later to find β_1.

It is expected that these values of β_o will overestimate ℓ_m, particularly for shock Mach numbers that are not large, due to the fact that the relative velocity between the wall and the free stream increases from $u_w - u_{e,o}$ at $\ell = 0$ to u_w at ℓ_m (compare Figs. 2a and 2b). Hence, the excess mass flow

in the boundary layer will be greater at a given ℓ than the excess obtained from the above model. This will result in smaller ℓ_m and larger β than obtained from Eq (7). However, for very strong shocks, where $u_{e,o}$ is small relative to u_w, Eq. (7) should give accurate results.

B. LOCAL SIMILARITY APPROXIMATION

In this subsection, the streamwise variation of free stream properties due to the increase in boundary layer mass flow with ℓ is taken into account. The development of the boundary layer and the variation in free stream properties are treated simultaneously. The boundary layer growth is found by assuming that at each station it is similar to a corresponding boundary layer developing in a uniform free stream behind a shock moving with uniform velocity (i.e., local similarity).

Since the flow is steady (Fig. 2a), the net mass flow through the shock equals the net mass flow at any station ℓ. Thus

$$A(\rho_e u_e)_o = A\rho_e u_e + L\int_o^\infty (\rho u - \rho_e u_e)\, dy \tag{8}$$

In Eq. (8), it is assumed that the boundary layer thickness is small compared with d; thus the integrand is nonzero only in the region close to the wall. Otherwise, for circular tubes, the coefficient L would have to be replaced by a factor $\pi(d - 2y)$ in the integrand of Eq. (8). Define

$$\bar{\delta} \equiv \frac{4}{d}\,\frac{\rho_e u_e}{(\rho_e u_e)_o}(-\delta^*) \tag{9}$$

where δ^* is the boundary layer displacement thickness based on the local free stream

$$\delta^* = \int_o^\infty \left(1 - \frac{\rho u}{\rho_e u_e}\right) dy \tag{10}$$

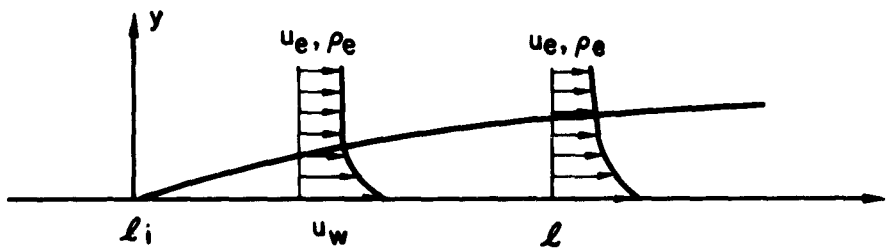

Fig. 3. Boundary Layer Development With Uniform Free Stream, Wall Velocity u_w, and Origin at ℓ_i

Note that $\bar{\delta}$ is the ratio of the excess mass flow through the boundary layer at ℓ to the mass flow through the shock. Thus $\bar{\delta}$ varies from 0 at $\ell = 0$ to 1 at $\ell = \ell_m$. Equations (8)-(10) then give

$$\bar{\delta} = 1 - \frac{\rho_e u_e}{(\rho_e u_e)_o} \tag{11}$$

which relates the free stream conditions to the local boundary layer displacement thickness.

The concept of local similarity is now introduced. It is assumed that the boundary layer profile at each ℓ corresponds to the profile for a boundary layer associated with a uniform free stream (equal to the local free stream) and a wall velocity u_w. The origin of this fictitious boundary layer is at ℓ_i, which is initially an unknown function of ℓ. (See Fig. 3.) The origin ℓ_i is chosen such that the excess flow in the boundary layer at each ℓ has the correct local value. If M_s is sufficiently large that variations in ρ_e and p_e can be ignored, Eqs. (11) and (A-11a) become

$$\bar{\delta} = 1 - V \tag{12a}$$

$$\bar{\delta} = H_e(\ell - \ell_i)^{4/5} \tag{12b}$$

where $V = u_e/u_{e,o}$ and H_e is a function of the local free stream as defined in Eq. (A-11b). The problem is now to solve these equations simultaneously to find $\bar{\delta}$ as a function of ℓ. The value of ℓ at $\bar{\delta} = 1$ defines ℓ_m and thus provides an improved estimate for β.

Assume that the local rate of growth of $\bar{\delta}$ follows the local similarity law $\bar{\delta} = H_e (\ell - \ell_i)^{1-n}$ (with H_e and ℓ_i considered constant at the local values). This is the approach used in Ref. 4. It follows that

$$\frac{\Delta\bar{\delta}}{\bar{\delta}} = (1-n)\,\frac{\Delta\ell}{\ell - \ell_i}$$

$$= (1-n)\left(\frac{H_e}{\bar{\delta}}\right)^{1/(1-n)} \Delta\ell \qquad (13)$$

For $n = 1/2$, this expression is the same as that derived in Ref. 4. For $n = 1/5$, Eqs. (13) and (12a) give, in integral form,

$$\ell = \frac{5}{4}\int_V^1 \frac{(1-V)^{1/4}}{H_e^{5/4}}\,dV \qquad (14)$$

Substituting Eq. (A-11b) for H_e and considering the limit $V = 0$, $\ell = \ell_m$ yields

$$\left(\frac{4K_o}{d}\right)^{5/4}\left(\frac{\nu_{w,o}}{u_w - u_{e,o}}\right)^{1/4}\ell_m = \frac{5}{4}\int_o^1 (1-V)^{1/4}\,\frac{W + BV}{W + B}\left(\frac{W-1}{W-V}\right)^2 dV \equiv F \qquad (15)$$

The constant B is defined in Appendix A. Equation (15) can not be integrated in closed form. For $W > 2$, F can be expressed as

$$F = 1 - 5\sum_{i=1}^{\infty} \frac{\dfrac{iB}{B+W} + \dfrac{i+1}{W-1}}{(5+4i)(1-W)^{i-1}} \qquad (16)$$

so that $F \to 1$, from below, as $W \to \infty$. Equation (15) has been numerically integrated for B = 7/3 and 2, which correspond to air and argon, respectively. The numerical results have been correlated to within 3 percent for $W \geq 1.5$ and to within 2 percent for $W \geq 2.0$ by the expression

$$F = \frac{W(W - 1)}{W^2 + 1.25W - 0.80} \tag{17}$$

Substitution of Eq. (15) into Eq. (5), to eliminate ℓ_m, yields the following value for β_1:

$$\beta_1 = \frac{\beta_o}{F^{4/5}} = \beta_o \left[\frac{W^2 + 1.25W - 0.80}{W(W - 1)}\right]^{4/5} \tag{18}$$

This expression has been used with the values of β_o in Table 2 to obtain corresponding values of β_1. These values are presented graphically in Fig. 4a.

C. NUMERICAL RESULTS FOR ℓ_m, Re_m, AND $2\delta_m/d$

The values of β_1 in Fig. 4a have been used to compute ℓ_m from Eq.(4). The results are given in Fig. 4b. Standard conditions were assumed to be $T_{st} = 522^{\circ}R$ and $p_{st} = 76$ cm Hg so that

$$\left(\frac{\rho a}{\mu}\right)_{st} = 6.93 \times 10^6 \text{ ft}^{-1} \quad \text{air} \tag{19a}$$

$$= 7.39 \times 10^6 \text{ ft}^{-1} \quad \text{argon} \tag{19b}$$

In order for the present theory to be valid, it is necessary that the boundary layer be turbulent. This will be the case if the Reynolds number at ℓ_m is considerably larger than the transition Reynolds number. An

Table 1. Numerical Constants Used to Obtain Results in Table 2 and Figure 4

$T_{st} = T_w = 522^{\circ}R$, $p_{st} = 1$ atm

Case	Gas	γ	σ	p_∞ cm Hg	r(0)	Sutherland Constant $^{\circ}R$	$\frac{\delta^*/\delta}{1 - W}$	B (Eq. A-10a)	$(\rho a/\mu)_{st}$ ft^{-1}
I	Ideal Argon	5/3	0.67	---	0.875	306	0.176	2	7.39×10^6
II	Ideal Air	7/5	0.72	---	0.897	198.6	0.157	7/3	6.93×10^6
III[a]	Real Air	---	0.72	0.5	0.897	198.6	0.157	7/3	6.93×10^6
IV[a]	Real Air	---	0.72	10	0.897	198.6	0.157	7/3	6.93×10^6

[a]Equilibrium normal shock solutions (Ref. 14) used for Cases III and IV.

Table 2. Values of β_o (Eq. 7)

Case I		Case II		Case III		Case IV	
M_s	β_o	M_s	β_o	M_s	β_o	M_s	β_o
1.41	0.0263	1.35	0.0253	6	0.0283	6	0.0270
1.73	0.0326	1.58	0.0332	8	0.0220	8	0.0210
2.24	0.0345	1.89	0.0389	10	0.0188	10	0.0175
3.00	0.0312	2.24	0.0413	12	0.0157	12	0.0149
3.46	0.0284	2.65	0.0413	14	0.0129	14	0.0122
4.12	0.0245	3.16	0.0391	16	0.0116	16	0.0106
5.20	0.0195	3.87	0.0348	18	0.0104	18	0.0095
6.08	0.0164	5.00	0.0282	20	0.0094	20	0.0084
7.55	0.0126	5.70	0.0248	--	---	--	---
8.77	0.0105	6.71	0.0208	--	---	--	---
10.82	0.0080	8.37	0.0161	--	---	--	---
---	---	9.75	0.0133	--	---	--	---

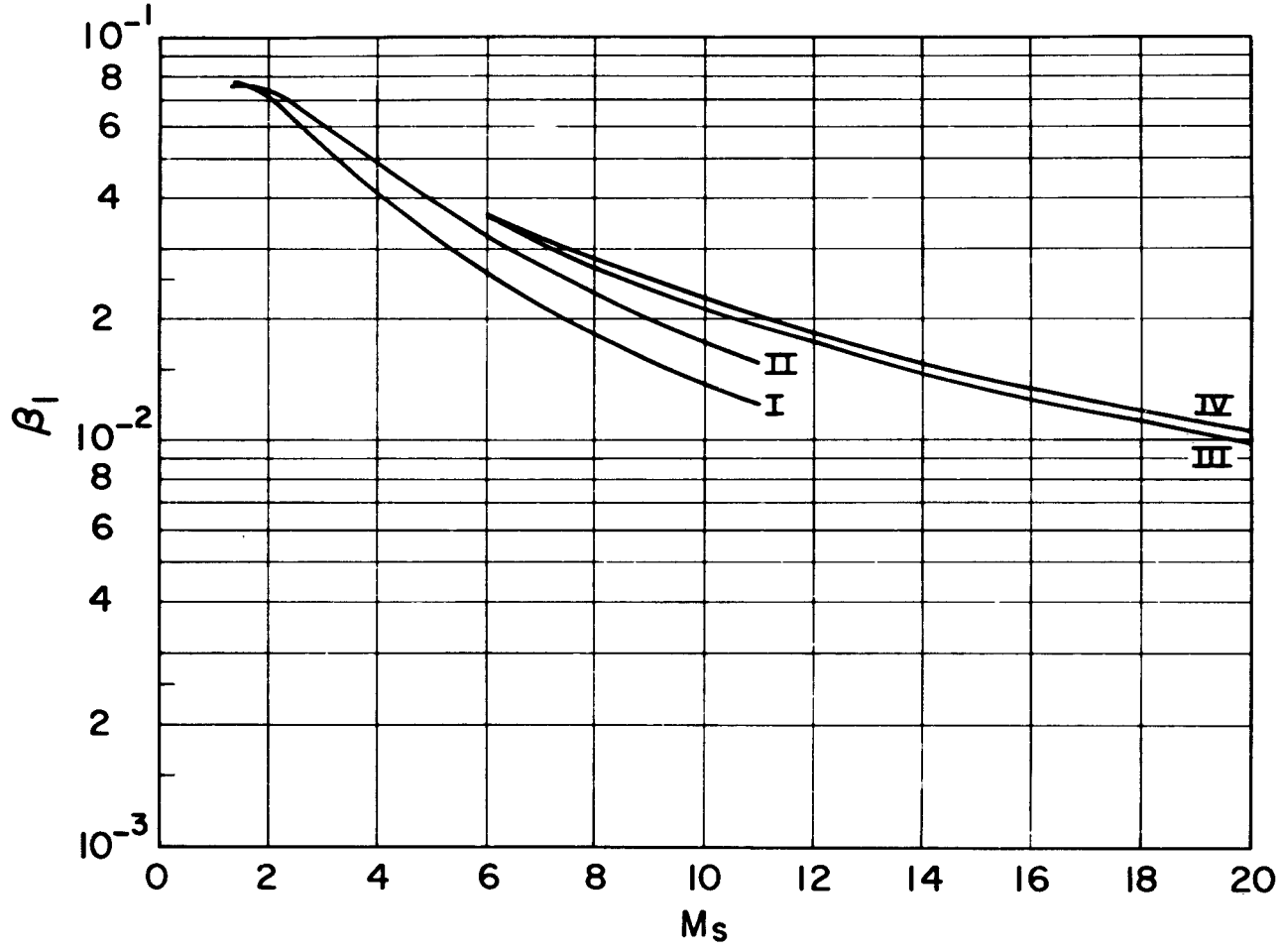

(a) β_1 Obtained from Eq. (18) and Table 2

Fig. 4. Quantities Defining Maximum Separation Distance for Turbulent Wall Boundary Layer. Cases I to IV Identified in Table 1

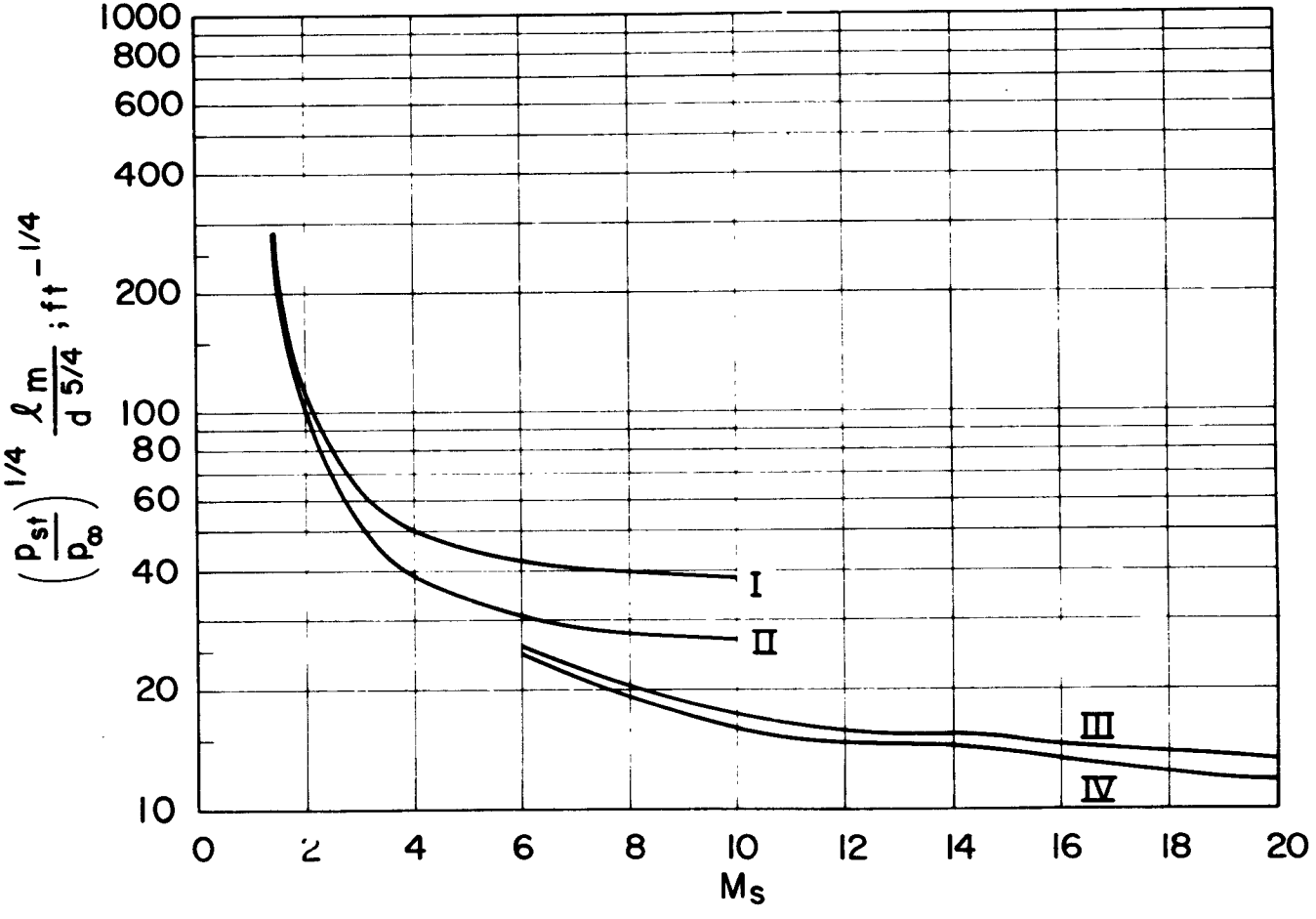

(b) Maximum Separation Distance ℓ_m Corresponding to β_1 (Eqs. 4, 18)

Fig. 4. (Continued)

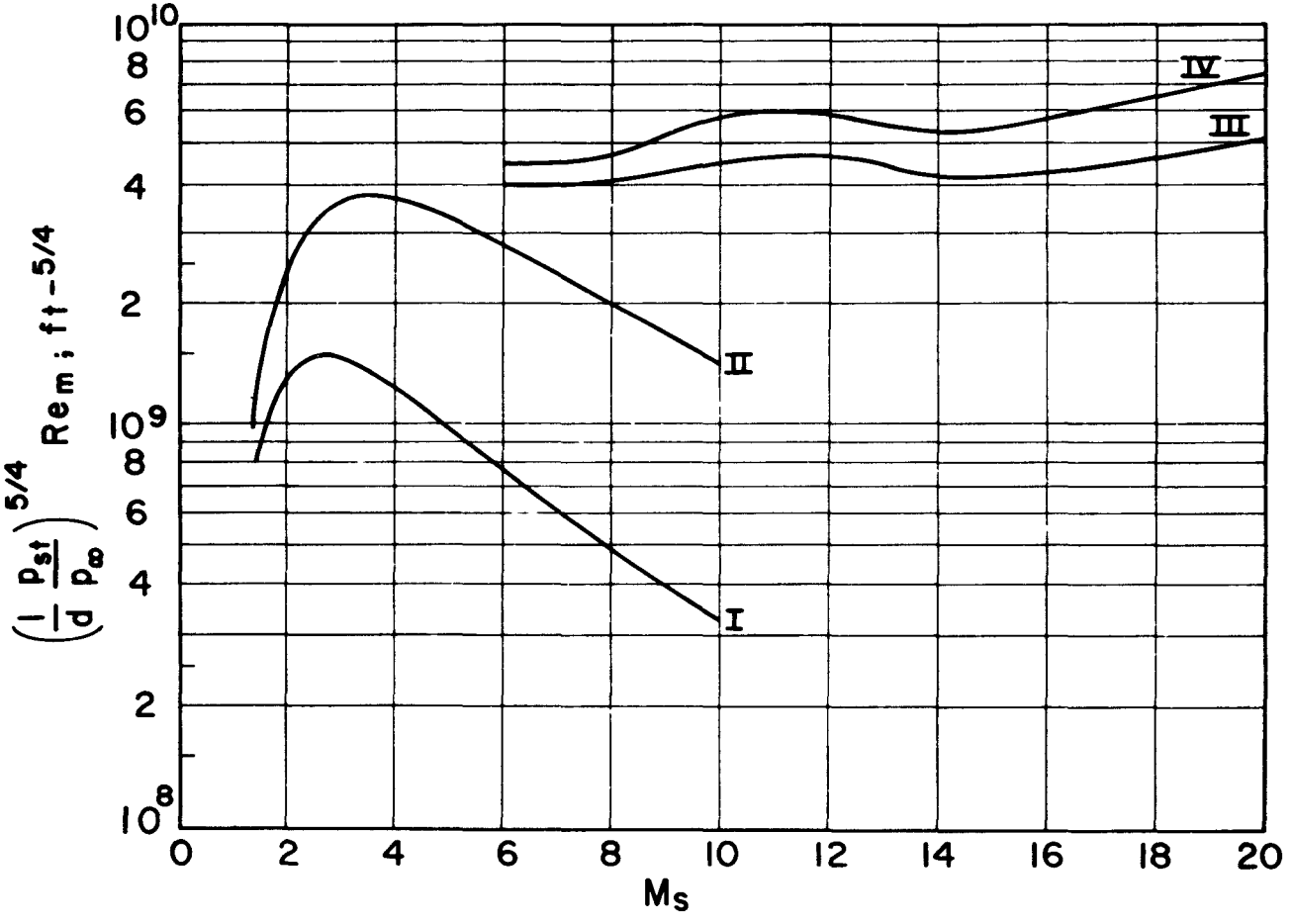

(c) Reynolds Number Corresponding to ℓ_m (Eq. 20)

Fig. 4. (Continued)

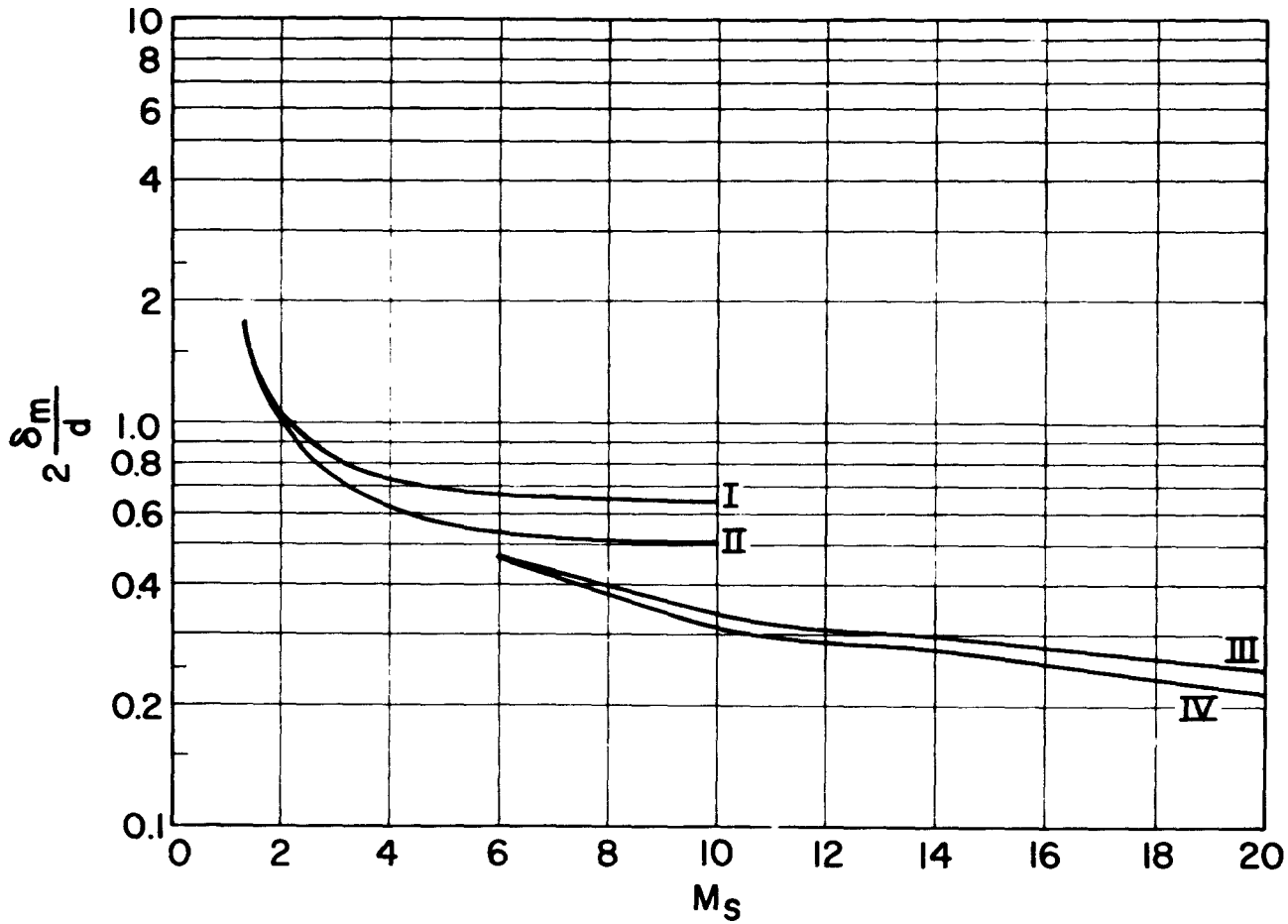

(d) Boundary Layer Thickness at ℓ_m (Eq. 21)

Fig. 4. (Continued)

appropriate Reynolds number, based on ℓ_m, is $Re_m = u_{e,o}(W - 1)^2 \ell_m / \nu_{e,o}$. A form convenient for calculation is

$$\left(\frac{l}{d}\frac{p_{st}}{p_\infty}\right)^{5/4} Re_m = (W - 1)^2 M_s \frac{\mu_\infty}{\mu_{e,o}} \left(\frac{\rho a}{\mu}\right)_{st} \left[\frac{\ell_m}{d^{5/4}}\left(\frac{p_{st}}{p_\infty}\right)^{1/4}\right] \tag{20}$$

This parameter is plotted in Fig. 4c. The transition Reynold's number has been investigated (Ref. 7) and is in the range $0.5 \leq Re_t \times 10^{-6} \leq 4$ for $1 \leq M_s \leq 9$. It appears to increase markedly for larger M_s, due to the stabilizing effect of the low wall temperatures, but only limited data are available. The present turbulent boundary layer theory should be applicable if Re_m is significantly larger than Re_t (say, $Re_m \geq 5\, Re_t$).

It has also been assumed (e.g., Eqs. 1, 8) that the boundary layer thickness is small relative to the tube radius. This condition will be satisfied if $2\delta_m/d$ is small. Here, δ_m is the boundary layer thickness at ℓ_m. If δ_m is assumed to vary as in the case of a uniform external stream, it can be shown that

$$\frac{2\delta_m}{d} = \frac{1}{2}\frac{F^{4/5}}{W - 1}\left(\frac{1 - W}{\delta^*/\delta}\right) \tag{21}$$

This parameter is plotted in Fig. 4d. It is seen that $2\delta_m/d \geq 1$ for $M_s \leq 2$ so that the assumption of a small boundary layer thickness is violated. For argon considered as an ideal gas (Case I), the quantity $2\delta_m/d$ doesn't go below 0.6; and for ideal air (Case II), it doesn't go below 0.45. The real gas solutions for air (Cases III, IV) have values below 0.5 for $M_s \geq 6$. However, it should be noted that $2\delta_m/d$ provides a very conservative estimate for the validity of the present theory. What is mainly required is that the boundary layer not become fully developed (i.e., $2\delta_m/d < 1$) and that the integrand in Eq. (8) not require the factor $\pi(d - 2y)$ (for circular cross sections). The

second of these conditions is probably satisfied when $2\delta_m/d < 1$ since most of the boundary layer excess mass flow occurs in the portion of the boundary layer near the wall. For example, by neglecting density effects and assuming a 1/7th power velocity profile, it can be shown that 56 percent of the excess mass flow occurs within a distance $\delta_m/4$ from the wall. The higher gas density at the wall (particularly for strong shocks) will considerably increase the fraction of excess mass flow in this distance. The present approach is therefore considered probably valid for $M_s \gtrsim 3$.

III. VARIATION OF SEPARATION DISTANCE WITH DISTANCE FROM DIAPHRAGM

In Section II, the limiting value of the separation distance between the shock and contact surface was found as a function of M_s. This value defines the test time in shock tubes that are sufficiently long to permit the separation limit to be reached. In order to estimate test times in shorter shock tubes, it is necessary to consider the rate at which separation distance increases with distance of the shock from the diaphragm. This problem is now discussed, using the approach in Ref. 4. It will be assumed that the shock moves with uniform velocity and that the flow between the shock and contact surface is steady in a shock-fixed coordinate system.

A. SEPARATION BETWEEN SHOCK AND CONTACT SURFACE

Consider flow in a coordinate system in which the shock is fixed and the wall moves with velocity u_w. Assume that at $t = 0$ the contact surface coincides with the shock, and at some later time, t, the portion of contact surface that is in the free stream is located at ℓ (Fig. 5). The problem is to find ℓ as a function of t. (In the present section, ℓ is considered a dependent variable defining the location of the contact surface relative to the shock as a function of time.)

For steady flow, the mass flow through the shock equals the mass flow through a control surface at ℓ. This yields an equation identical to Eq. (11), namely,

$$\overline{\delta} = 1 - \frac{\rho_e u_e}{(\rho_e u_e)_o} \tag{11}$$

where $\overline{\delta}$ is again the ratio of the excess boundary layer mass flow at ℓ to the mass flow through the shock. For the present purposes it can be assumed that the excess mass flow in the boundary layer varies as ℓ^{1-n}. Then,

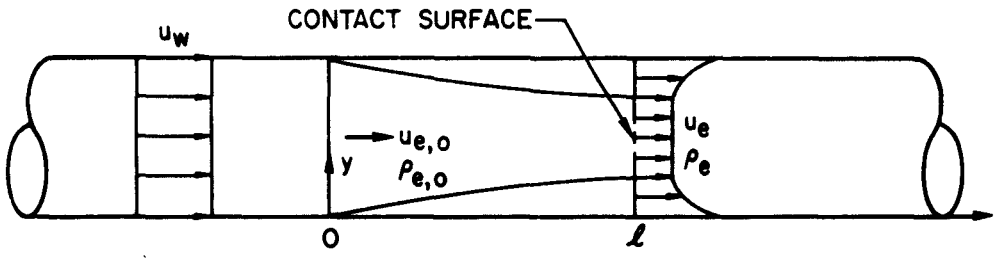

Fig. 5. Flow Model for Finding Separation Distance Between Shock and Contact Surface as a Function of Time

$\overline{\delta} = (\ell/\ell_m)^{1-n}$. Also, it will be assumed that $\rho_e/\rho_{e,o} = 1$ (valid for strong shock). These assumptions have been shown to be accurate (Ref. 4), except near W = 1 where the present solution for ℓ_m is invalid anyway. Equation (11) then becomes

$$\left(\frac{\ell}{\ell_m}\right)^{1-n} = 1 - \frac{u_e}{u_{e,o}} \tag{22}$$

Introduce the nondimensional variables

$$X \equiv \frac{u_{e,o}\, t}{\ell_m} \equiv \frac{x_s}{W\ell_m} \tag{23a}$$

$$T \equiv \frac{\ell}{\ell_m} \tag{23b}$$

where $x_s = u_w t$ is the distance of the shock from the diaphragm in laboratory coordinates (Fig. 6). Noting that $d\ell/dt = u_e$, write Eq. (22) in the form

$$T^{1-n} = 1 - \frac{dT}{dX} \tag{24}$$

Integrating,

$$X = \int_o^T \frac{dT}{1 - T^{1-n}} \tag{25}$$

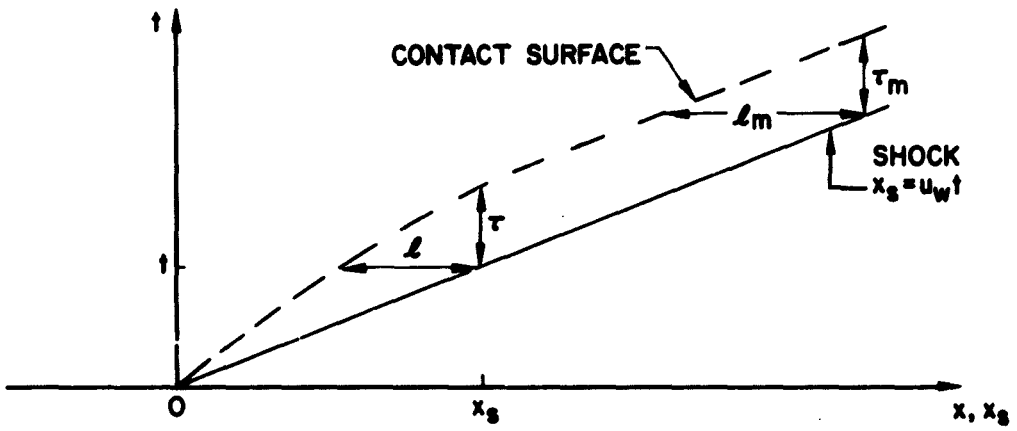

(a) t-x Diagram

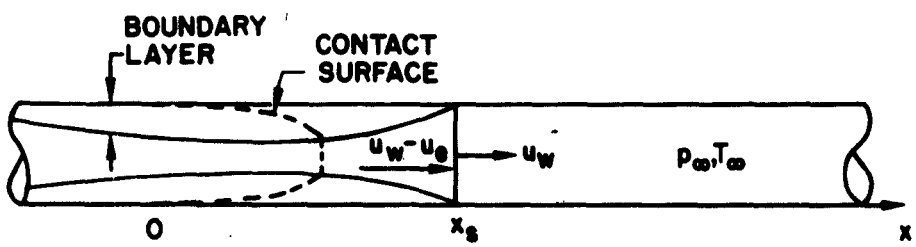

(b) Shock Tube

Fig. 6. Flow in Laboratory Coordinates Assuming Shock Has Uniform Velocity

Thus,

$$-\frac{X}{2} = \ln(1 - T^n) + T^n \qquad \text{for } n = 1/2 \qquad (26a)$$

$$= \frac{5}{8}\left(\ln\frac{1 - T^n}{1 + T^n} - 2\tan^{-1} T^n + 4T^n\right) \qquad \text{for } n = 1/5 \qquad (26b)$$

Equation (26a) was first derived by Roshko.*

The variation of T with X is tabulated in Table 3 and is plotted in Fig. 7 for n = 1/2, 1/5. Note that T = X corresponds to an ideal (no boundary layer) shock tube. The departure of the curves in Fig. 7 from T = X represents the departure from ideal performance. For $X \lesssim 0.1$, the departure is small, and for $X \gtrsim 10$, the separation distance equals the limiting value. Note that ℓ equals 59 percent of the ideal value when X = 1, n = 1/5.

B. TEST TIME

In the previous subsection, the separation distance was obtained as a function of t. A quantity that is perhaps of greater interest is the test time (i.e., the difference in time between the arrival of the shock and the arrival of the contact surface) at a fixed distance from the diaphragm, x_s. This quantity will now be discussed.

Designate the test time by τ. For $x_s \to \infty$, $\tau \equiv \tau_m = \ell_m/u_w$. Define $\bar{\tau} \equiv \tau/\tau_m$, which is the test time at x_s divided by the test time at $x_s \to \infty$. If it is assumed that the shock moves with constant velocity, X and $\bar{\tau}$ are related (Ref. 4) by

$$X = X_b - (T_b/W) \qquad (27a)$$

*Equation (26b) was derived by Dr. E. F. Brocher in an as yet unpublished study of test time for the case of small departures from the ideal flow.

Table 3. Variation of T with X (Eq. 25)

T	X	
	n = 1/2	n = 1/5
0.01	0.0107	0.0101
0.05	0.0590	0.0527
0.10	0.128	0.110
0.20	0.291	0.238
0.30	0.491	0.388
0.40	0.737	0.564
0.50	1.04	0.776
0.60	1.43	1.04
0.70	1.95	1.39
0.80	2.71	1.88
0.90	4.04	2.73
0.92	4.48	3.01
0.94	5.04	3.37
0.96	5.84	3.87
0.98	7.22	4.73
0.99	8.60	5.60

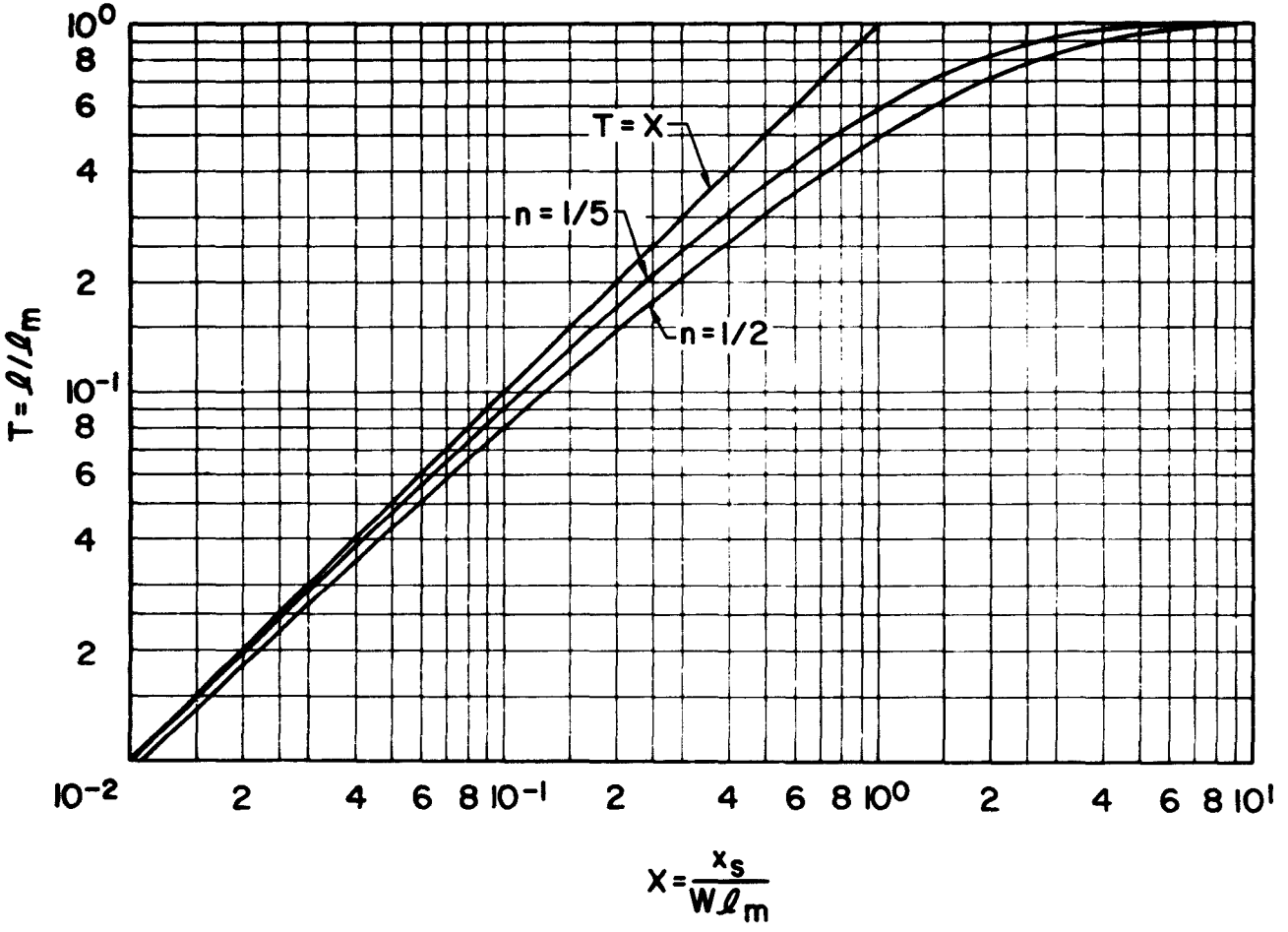

Fig. 7. Separation Distance as a Function of Distance from Diaphragm (Table 3)

$$\bar{\tau} = T_b \tag{27b}$$

where X_b, T_b are corresponding values from Table 3. The variation of $\bar{\tau}$ with X is plotted in Fig. 8a for W = 2, 4, 8, ∞.

An analytical expression relating T and $\bar{\tau}$ can be found as follows. Assume that the contact surface velocity is constant during the period of time between the arrival of the shock and the arrival of the contact surface at x_s. The test time would then equal $\tau = \ell/(u_w - u_e)$, or, from Eq. (22),

$$\bar{\tau} = \frac{WT}{W - 1 + T^{1-n}} \tag{27}$$

At the start of the motion, $\bar{\tau} = WT/(W - 1)$. After long times, $\bar{\tau} = T = 1$. For large W, $\bar{\tau} = T$ for the entire motion.

The parameter $\bar{\tau}$ compares the test time τ to the asymptotic test time ℓ_m/u_w. It is also of interest to compare τ to the test time for an ideal shock tube, τ_i. The ideal test time at a distance x_s from the diaphragm is

$$\tau_i = x_s/(u_w - u_{e,o})W$$

The actual time, assuming u_e is constant between arrival of shock and contact surface, can then be expressed as

$$\frac{\tau}{\tau_i} = \frac{T}{X}\,\frac{W - 1}{W - 1 + T^{1-n}} \tag{28}$$

This is plotted in Fig. 8b for n = 1/5 and W = 2, 4, 8, ∞. For large W, $\tau/\tau_i = T/X$. Note that when X = 1, the test time is about 1/2 of the ideal value. The ratio τ/τ_i equals $(W - 1)/WX$ for $X \gtrsim 5$.

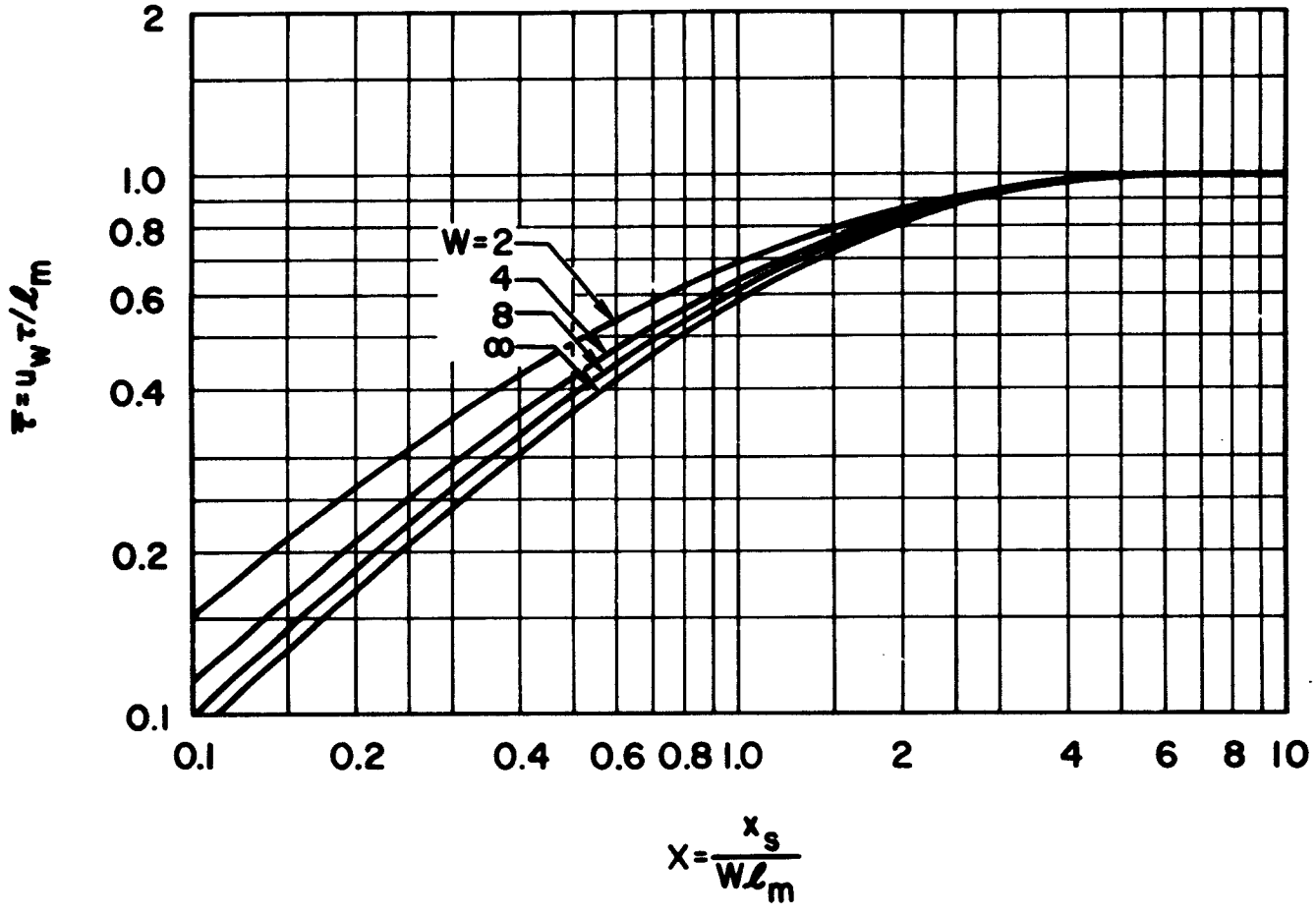

(a) Normalized by Maximum Possible Test Time ℓ_m/u_w

Fig. 8. Test Time as a Function of Distance from Diaphragm, n = 1/5

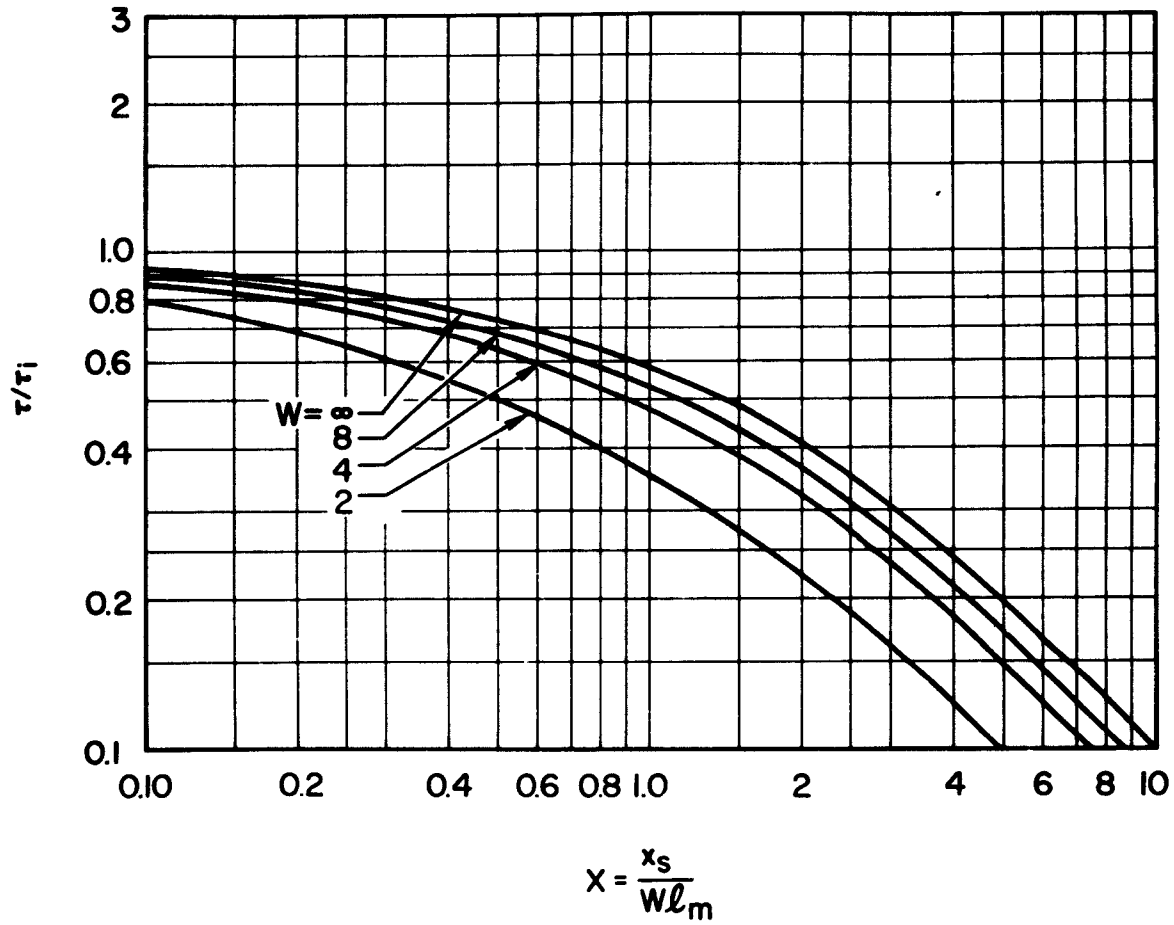

(b) Normalized by Ideal Test Time τ_i

Fig. 8. (Continued)

IV. COMPARISON WITH ANDERSON'S SOLUTION

There is a basic difference between the separation distance solution presented by Anderson (Ref. 5) and the one presented in this paper. Anderson's method for finding the separation distance corresponding to a given shock location, x_s, is as follows. He assumes that the shock moves with uniform velocity, and finds the separation distance by equating $A\ell\rho_{e',o}$ to the difference between the ideal amount of shocked gas, $Ax_s\rho_\infty$, and the amount of gas that has slipped past the contact surface. The latter he finds, incorrectly, to be of the form $K_1 A\rho_\infty x_s^{9/5}$ (assuming a thin boundary layer) where K_1 is a function of M_s, d, p_∞, and is tabulated by Anderson. The separation distance is then

$$\ell = \frac{\rho_\infty}{\rho_{e,o}} x_s \left(1 - K_1 x_s^{4/5}\right)$$

It is seen that as x_s increases, ℓ first increases, reaches a maximum at a finite value of x_s [namely, $x_s = (5/9\ K_1)^{5/4}$], and then decreases. In the present solution, ℓ increases monotonically with x_s and asymptotically approaches ℓ_m as $x_s \to \infty$. Hence the two solutions have different behaviors.

Anderson's expression for the net mass loss past the contact surface is based on the ideal separation distance between shock and contact surface. It can be readily shown that his estimate is too large, except for small x_s. If the free stream is assumed to remain uniform, the mass flow past the contact surface at any instant is proportional to $\ell^{4/5}$. The net mass loss since the start of the motion for a shock moving with uniform velocity is proportional to

$$\int_o^{x_s} \ell^{4/5}\, dx_s$$

For small x_s, where ℓ varies linearly with x_s, the net mass loss has the form $x_s^{9/5}$, as derived by Anderson. For large x_s, ℓ approaches ℓ_m, and the net mass loss tends to become proportional to $\ell_m^{4/5} x_s$, which is considerably smaller than the $x_s^{9/5}$ dependence used by Anderson. Thus, Anderson's solution overestimates the mass loss and underestimates the test time for large x_s. This accounts for the differences in the behavior of the two solutions.

For moderate values of x_s, say $x_s \lesssim (5/9K_1)^{5/4}$, it is difficult to predict how Anderson's numerical results will compare with ours. Note that the present theory includes the interaction between the boundary layer and the inviscid flow (β_1 solution), which reduces the predicted test time as compared with a non-interaction theory (β_0 solution and Anderson's solution). Anderson's overestimation of mass loss tends to compensate for his neglect of the boundary layer-free stream interaction, at least for moderate x_s.

In Anderson's illustrative examples, $M_s = 6$; $p_\infty = 10$ cm Hg; $d = 3/2$ in.; $x_s = 15$ ft; and $d = 4$ in.; $x_s = 50$ ft. His theory predicted about 50 percent of ideal test time. The present theory predicts about 30 percent of ideal test time for these cases. Thus, in these examples, Anderson predicts more test time than does the present theory. However, with increase in x_s, his theory must eventually predict lower values.

V. DISCUSSION

The present results can be used to estimate shock tube test time reduction due to mass loss to a turbulent wall boundary layer. The procedure is as follows. First, Re_m is found from Fig. 4b for given M_s, d, and p_∞. If this is substantially larger than Re_t (say $Re_m \geq 5\ Re_t$), the limiting separation between shock and contact surface will be due mainly to a turbulent boundary layer. Hence the turbulent boundary layer analysis can be used to estimate major reductions in shock tube test time. Next, ℓ_m is found from Fig. 4b and the value of $X = x_s/W\ell_m$ can be determined for a given test section distance from the diaphragm. Finally, the test time can be found from Figs. 8.

If Re_m, based on a laminar boundary layer, is less than Re_t, laminar boundary layer theory is applicable and a similar procedure is followed using the corresponding curves in Ref. 4.

The parameter that primarily determines Re_m is dp_∞. For a given value of dp_∞, the length-to-diameter ratio, x_s/d, determines the amount of test time reduction. Typical values for these quantities can be obtained from Figs. 9 and 10, for turbulent and laminar flows, respectively. These figures are based on the identities

$$Re_m = \left[Re_m\left(\frac{1}{d}\frac{p_{st}}{p_\infty}\right)^{1/(1-n)}\right]\left(d\frac{p_\infty}{p_{st}}\right)^{1/(1-n)} \tag{29a}$$

$$\frac{x_s}{Xd} = W\left[\frac{\ell_m}{d^{1/(1-n)}}\left(\frac{p_{st}}{p_\infty}\right)^{n/(1-n)}\right]\left(d\frac{p_\infty}{p_{st}}\right)^{n/(1-n)} \tag{29b}$$

where the terms in square brackets have been evaluated for both laminar (Ref. 4) and turbulent wall boundary layers (Fig. 4).

Values of Re_m are plotted versus M_s for fixed values of dp_∞ in Figures 9a and 10a; the product dp_∞ has the units (in.) (cm Hg). Also plotted in these figures are estimated values of Re_t and $5\,Re_t$. (It was assumed that Re_t varies linearly on the loglog plot from $Re_t = 0.5 \times 10^6$ at $M_s = 1$ to $Re_t = 4 \times 10^6$ at $M_s = 9$. The curves are not continued beyond $M_s = 9$ because of uncertainty in Re_t.) Turbulent boundary layer theory is applicable for values of dp_∞ that result in $Re_m \gtrsim 5\,Re_t$. These values (from Fig. 9a) are

air	argon
$dp_\infty \geq 4$ for $M_s = 3$	$dp_\infty \geq 2$ for $M_s = 3$
$dp_\infty \geq 10$ for $M_s = 8$	$dp_\infty \geq 10$ for $M_s = 8$

Similarly, laminar boundary layer theory is applicable when $Re_m \lesssim Re_t$, or (from Fig. 10a) when

air	argon
$dp_\infty \leq 0.3$ for $M_s = 3$	$dp_\infty \leq 0.6$ for $M_s = 3$
$dp_\infty \leq 0.3$ for $M_s = 8$	$dp_\infty \leq 1$ for $M_s = 8$

It follows that, roughly, turbulent theory applies for $dp_\infty \gtrsim 5$ and laminar theory applies for $dp_\infty \lesssim 0.5$, for $3 \leq M_s \leq 9$.

In Figures 9b and 10b x_s/Xd is plotted versus M_s for various dp_∞. The ordinate may be viewed as the value of x_s/d corresponding to $X = 1$; that is, the length-to-diameter ratio that results in about 1/2 the ideal test time. For air or argon turbulent boundary layers and $M_s > 3$, $x_s/Xd \approx 45$, 80, 140 for $dp_\infty \approx 5$, 50, 500. (Thus, a shock tube with $dp_\infty \approx 5$ and $x_s/d \approx 50$ will have about half the ideal test time). Similarly, for air or argon laminar boundary layers, Fig. 10b shows $x_s/Xd \approx 100$, 10, and 1 for $dp_\infty \approx 0.5$, 0.05, and 0.005, respectively.

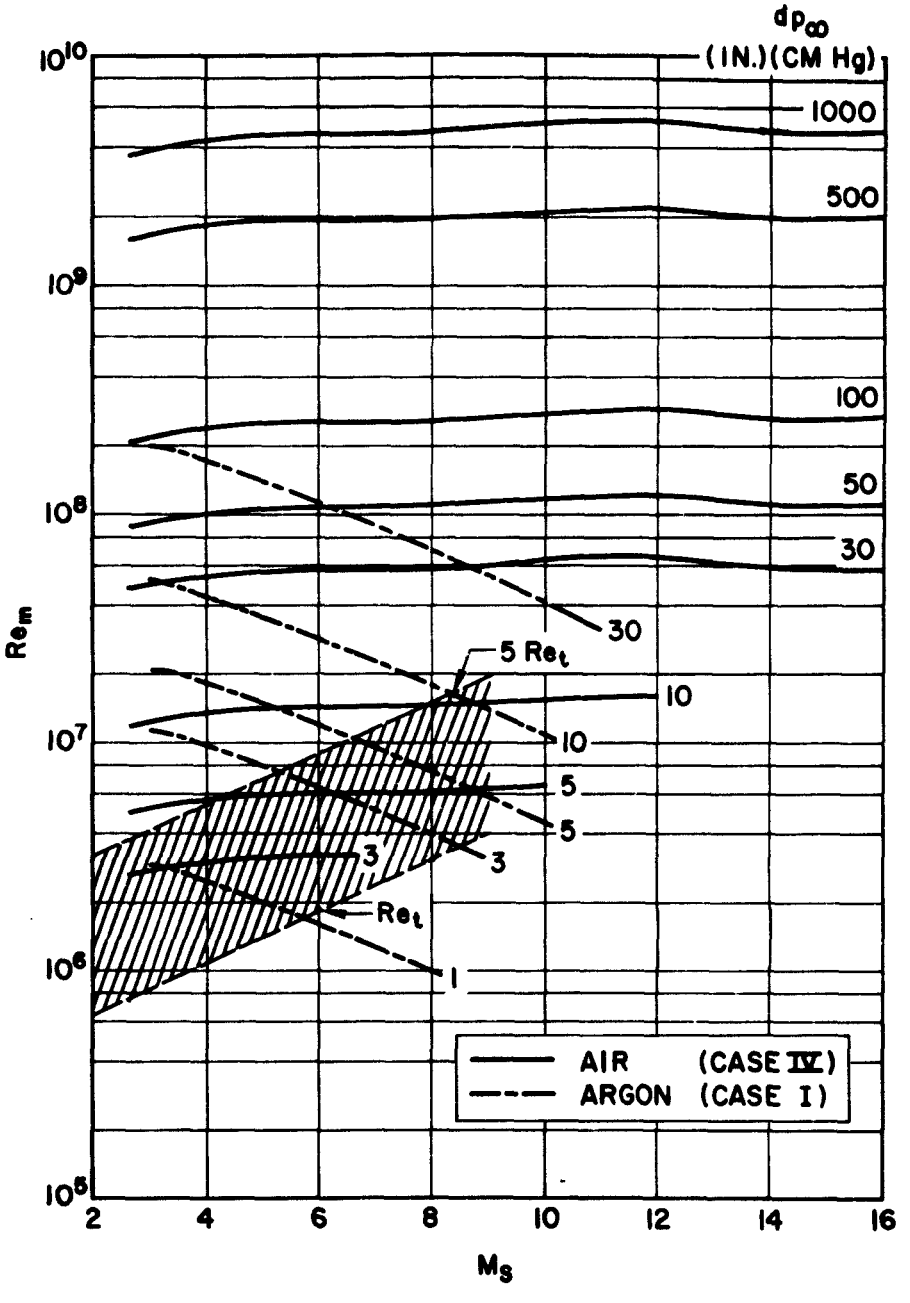

(a) Re_m

Fig. 9. Dependence of Re_m and x_s/dX on M_s and dp_∞ for Turbulent Boundary Layer

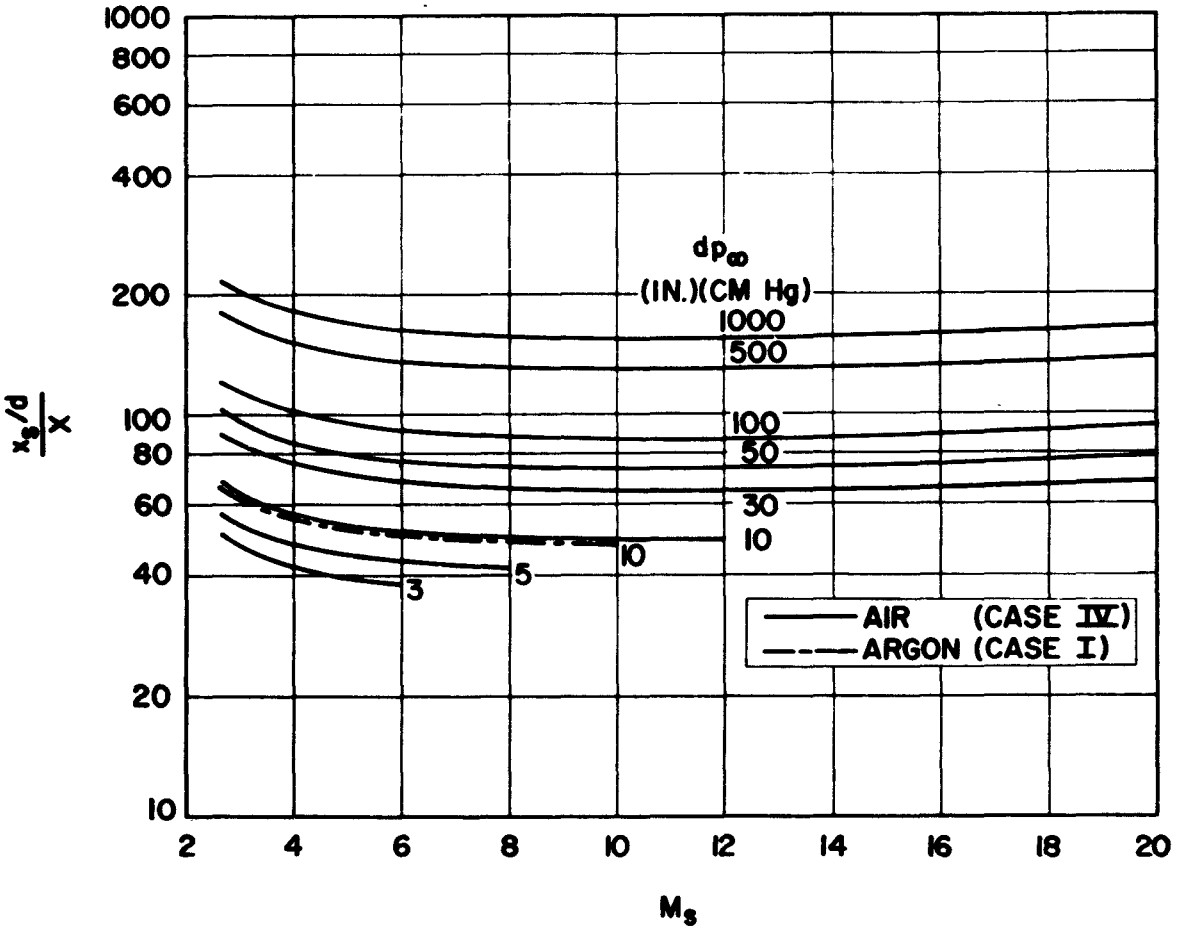

(b) x_s/dX

Fig. 9. (Continued)

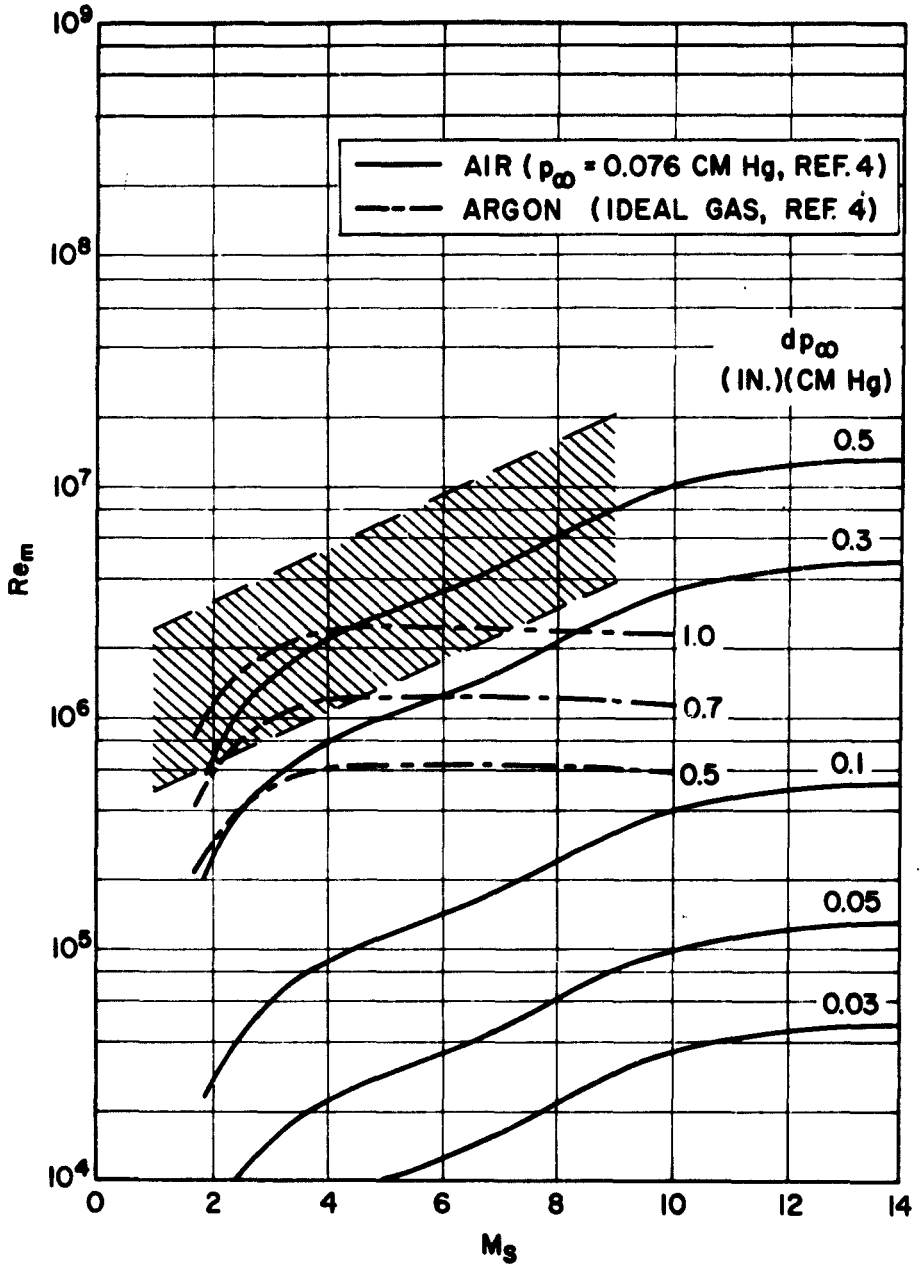

(a) Re_m

Fig. 10. Dependence of Re_m and x_s/dX on M_s and dp_∞ for Laminar Boundary Layer

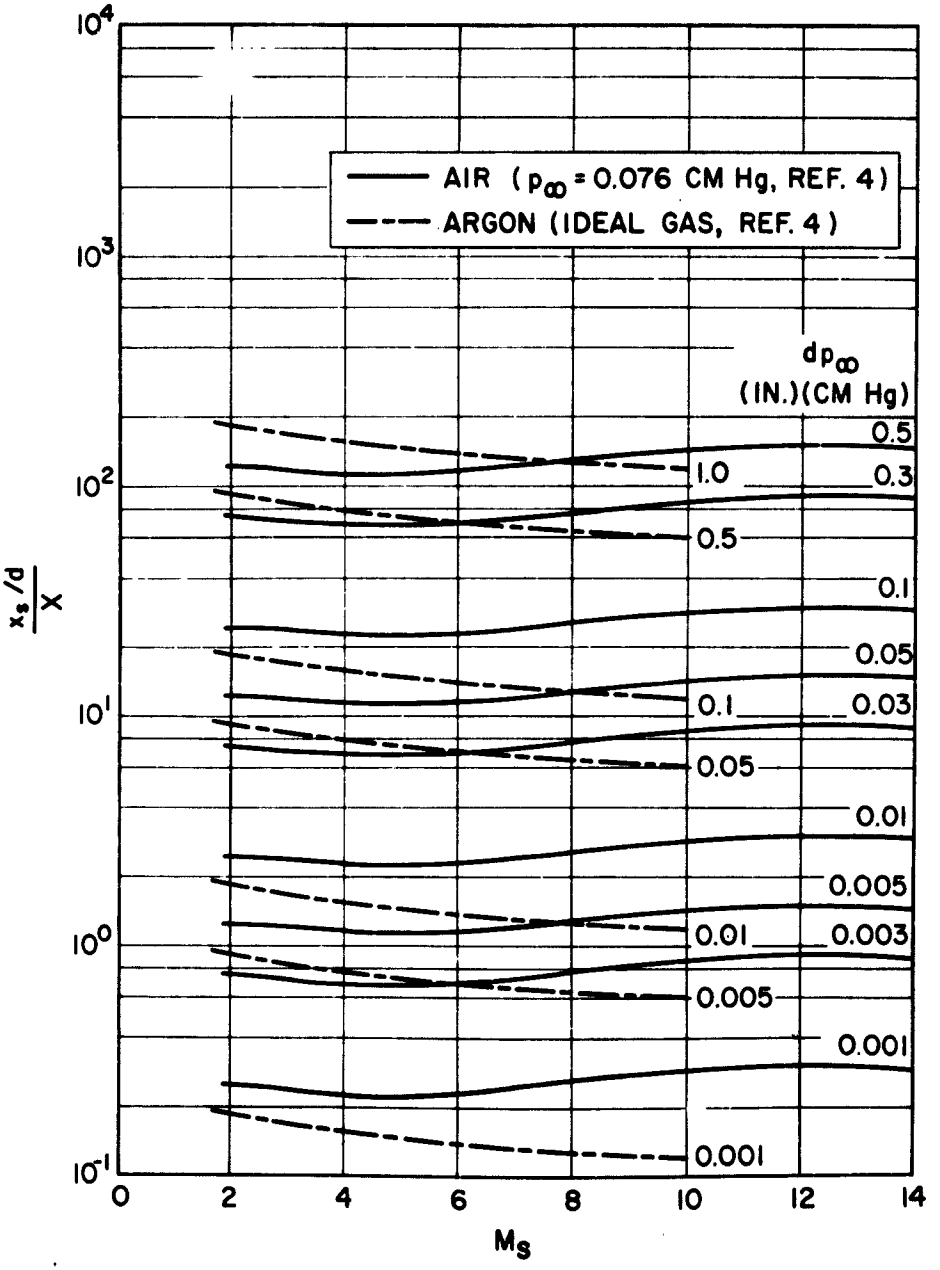

(b) x_s/dX

Fig. 10. (Continued)

These numerical results are intended to give an indication of when turbulent or laminar theory applies, and rough estimates of the test time limitation. More accurate estimates are made from Figs. 4 and 8.

Before the present generation of low pressure shock tubes,* the typical low pressure section of a shock tube had an internal diameter in the range 1 in. $\leq d \leq$ 4 in. and a length-to-diameter ratio in the range 40-150 (Ref. 8). Longer tubes were sometimes used, particularly in studies of shock attenuation; for example, a 2-in. × 40-ft tube ($x_s/d = 240$) was used in Ref. 9, and a 3.75-in. × 120-ft tube ($x_s/d = 384$) in Ref. 10.

In a given shock tube, the largest reduction in test time, due to a wholly turbulent boundary layer, occurs at $dp_\infty \approx 5$ (in.) (cm Hg), for which $x_s/Xd \approx 45$. Tubes with $x_s/d \approx 45$ will have $X = 1$, or around half the theoretical test time (see Fig. 8b). Tubes with $x_s/d \approx 150$ will have $X \approx 3$, or around 1/4 of the ideal test time. (The 40 percent lower limit on test time, noted in Ref. 6 and discussed in Section I, is therefore not sufficiently low for this case). With regard to the larger values of x_s/d considered in Refs. 9 and 10, it might be noted that $X \approx 5.5$ for $x_s/d = 240$ and $X \approx 8.5$ for $x_s/d = 384$. Here, the test times are approximately 0.15 and 0.1 of the ideal values, respectively. For these values of X, the separation distance has reached its maximum value (Fig. 7).

The smallest reduction in test time, due to a wholly laminar boundary layer, occurs when $dp_\infty \approx 0.5$. From the results given in Ref. 4, it can be seen that the test time is about 1/2 the ideal value when $x_s/d \approx 100$. The test time is slightly larger than the corresponding value for a turbulent boundary layer with $dp_\infty \approx 5$.

*Present day low pressure tubes have low pressure sections: 6 in. × 30 ft (AVCO), 24 in. × 50 ft (AVCO), 17 in. × 36 ft (Aerospace), 17 in. × 70 ft (Caltech).

It is thus seen that, for a given shock tube, operation at an initial pressure such that $dp_\infty \approx 5$ results in a <u>local</u> minimum in the maximum possible test time. Higher values of dp_∞ will result in thinner turbulent boundary layers and therefore more test time. With a decrease in dp_∞, the onset of a wholly laminar boundary will first tend to increase the test time; however, with further decrease in dp_∞, the boundary layer mass flow will increase and severe test time limitations will occur.

VI. CONCLUDING REMARKS

The effect of wholly laminar and wholly turbulent wall boundary layers on shock tube test time has been discussed. It has been shown that, for given shock Mach number, the maximum test time, τ_m, and separation distance, ℓ_m, depend primarily on

$$\tau_m \sim \ell_m \sim d(dp_\infty)^{n/(1-n)} \sim d^2 p_\infty \qquad \text{for } n = 1/2$$

$$\sim d^{5/4} p_\infty^{1/4} \qquad \text{for } n = 1/5$$

Since the ideal test time, τ_i, is proportional to distance from the diaphragm, x_s, it also follows that

$$\tau_m/\tau_i \sim \frac{d}{x_s}\, dp_\infty \qquad \text{for } n = 1/2$$

$$\sim \frac{d}{x_s}\, (dp_\infty)^{1/4} \qquad \text{for } n = 1/5$$

These equations show that the maximum test time is proportional to p_∞ for laminar flows and to $p_\infty^{1/4}$ for turbulent flows. Hence the laminar wall boundary layer case is more sensitive to p_∞.

Examples of previous studies have been noted where turbulent wall boundary layers have reduced the test time from 0.1 to 0.5 of the ideal value. The rule-of-thumb (see Section I) that assumes about one half of the ideal test time to be actually available is therefore not dependable. The methods outlined herein should be used to estimate test time when necessary.

It should be kept in mind that the present calculations actually provide an upper limit on the test time. It is also necessary to consider (a) non-ideal diaphragm rupture (which promotes interface mixing and causes non-ideal flow near the diaphragm) and (b) flow nonuniformity between the shock and contact surface. When the maximum separation is reached, the flow nonuniformity between the shock and contact surface can be estimated from Eq. (22) by assuming steady isentropic flow in a shock-fixed coordinate system.

It should also be noted that the validity of the turbulent boundary layer theory used in the present report has not been established for strong shocks (see Appendix A). The present results are therefore intended as a first estimate for the effect of turbulent boundary layers on shock tube test time. Experimental confirmation of these results would be desirable.

APPENDIX A

Turbulent Boundary Layer Behind Moving Shock

The turbulent boundary layer behind a moving shock was analytically studied in Refs. 11 and 12. The general validity of some of the analytical results given in Refs. 11 and 12 was experimentally established in Refs. 13 and 7 for Mach numbers up to about 3 and 6, respectively. Higher Mach numbers were not studied therein; hence the accuracy of the results in Refs. 11 and 12 has not been fully established, particularly for strong shocks ($M_s > 6$). Nevertheless, the results in Refs. 11 and 12 for displacement thickness will be summarized here and put in a form suitable for studying test time in shock tubes. This will provide at least a first estimate of the effect of turbulent wall boundary layers on shock tube test time.

Assume that a shock moves with constant velocity, that the inviscid flow behind the shock is uniform, and that the wall boundary layer is turbulent (Fig. 2a). The variation of displacement thickness with distance behind the shock (from Refs. 11, 12) is

$$-\delta^* \equiv \int_0^\infty \left[\frac{\rho u}{(\rho_e u_e)_o} - 1\right] dy$$

$$\equiv K_o \ell^{4/5} \left(\frac{\nu_{w,o}}{u_w - u_{e,o}}\right)^{1/5} \qquad \text{(A-1)}$$

where

$$K_o \equiv 0.0575 \frac{\delta^*/\delta}{1 - W}\left(\frac{1 - W}{\theta/\delta}\right)^{4/5} (W - 1)^{9/5} \left[\frac{\mu_m}{\mu_w} \frac{\rho_w}{\rho_{e,o}} \left(\frac{\rho_m}{\rho_{e,o}}\right)^3\right]^{1/5} \qquad \text{(A-2)}$$

Here, δ is the boundary layer thickness, and θ the momentum thickness. The subscript m refers to conditions evaluated at a mean reference static enthalpy defined by

$$\frac{h_m}{h_{e,o}} = 0.5\left(\frac{h_w}{h_{e,o}} + 1\right) + 0.22\left(\frac{h_r}{h_{e,o}} - 1\right) \qquad \text{(A-3)}$$

where h_r is the recovery enthalpy (i.e., the wall value of h for which there is no heat transfer).

In order to find K_o, it is necessary to evaluate $(\delta^*/\delta)/(1 - W)$ and $(\theta/\delta)/(1 - W)$, which are functions of W, $h_r/h_{e,o}$, and $h_w/h_{e,o}$ that can be found from

$$\frac{\delta^*/\delta}{1 - W} = \frac{1}{W - 1}\left\{7\,\frac{h_{e,o}}{h_w}\int_o^1 \frac{\zeta^6[W - (W - 1)\zeta]}{1 + b\zeta - c\zeta^2}\,d\zeta - 1\right\} \qquad \text{(A-4a)}$$

$$\frac{\theta/\delta}{1 - W} = 7\,\frac{h_{e,o}}{h_w}\int_o^1 \frac{\zeta^6[W - (2W - 1)\zeta + (W - 1)\zeta^2]}{1 + b\zeta - c\zeta^2}\,d\zeta \qquad \text{(A-4b)}$$

where

$$b = \frac{h_r}{h_w} - 1 \qquad c = \frac{h_r}{h_w} - \frac{h_{e,o}}{h_w} \qquad \text{(A-5)}$$

[In reviewing the work of Refs. 11 and 12, it appears that for strong shocks it might be advisable to replace $h_{e,o}/h_w$ and h_r/h_w in Eqs. (A-4) and (A-5) by $\rho_w/\rho_{e,o}$ and ρ_w/ρ_r, respectively. However, this point will not be pursued.] Equation (A-4) can be evaluated for given b, c, and W, using the

tables presented in Refs. 10 and 11. For strong shocks, these tables require taking the differences of large, nearly equal numbers; thus the accuracy is reduced. (Approximate expressions for evaluating Eqs. (A-4) for strong shocks are given in Appendix B.) If convenient, it is preferable to evaluate δ^*/δ and θ/ζ by the numerical integration of Eq. (4).

Ideal Gas

Eqs. (A-4) and (A-2) can be evaluated as a function of M_s for gases with constant specific heat ratios, γ, obeying the perfect gas laws, $p = \rho RT$ and $h = c_p T$. For these gases,

$$\frac{h_r}{h_{e,o}} = 1 + \frac{(W - 1)^2}{ZW - 1} r(0) \qquad \text{(A-6a)}$$

$$\frac{h_w}{h_{e,o}} = \frac{W(Z - W)}{ZW - 1} \qquad \text{(A-6b)}$$

where $Z = (\gamma + 1)/(\gamma - 1)$, and $r(0) = (\sigma)^{1/3}$ is the recovery factor (σ = Prandtl number). Eq. (A-6a) follows from the definition of recovery factor, and Eq. (A-6b) is a normal shock relation. The latter assumes that the wall temperature is the same as the gas temperature upstream of the shock.

Equations (A-4) have been evaluated for $\gamma = 7/5$, $r(0) = 0.897$ and for $\gamma = 5/3$, $r(0) = 0.875$. These values correspond to ideal air and to ideal argon, respectively. The cases $\gamma = 7/5$, $r(0) = 1$ and $\gamma = 5/3$, $r(0) = 1$ have also been evaluated to find the effect of $r(0)$. The results are given in Fig. 11 and can be approximated by the following expressions.

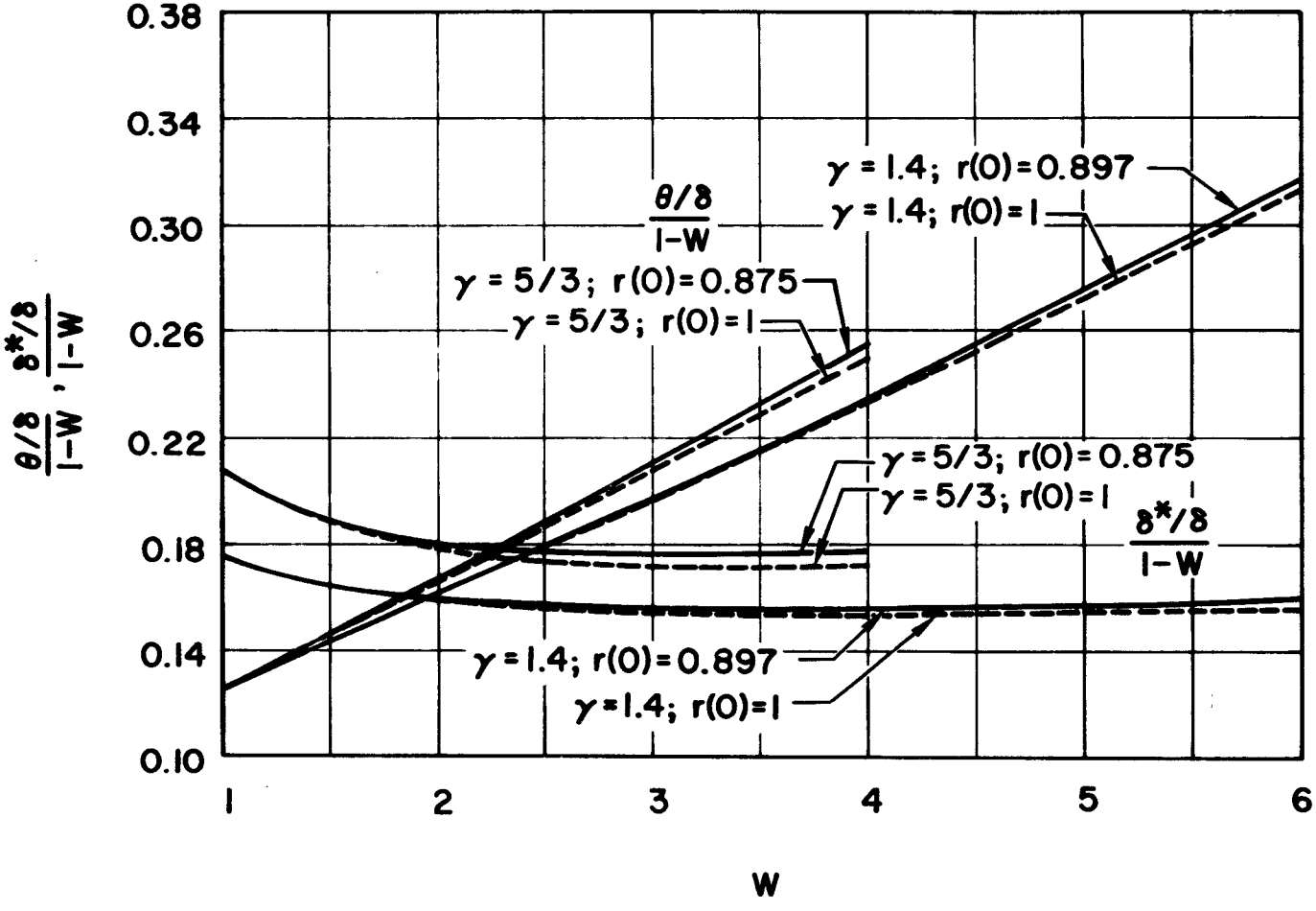

Fig. 11. Turbulent Boundary Layer Displacement and Momentum Thicknesses, Ideal Gas

$$\frac{\theta/\delta}{1 - W} \equiv \frac{W + B}{C} = \frac{W + (7/3)}{80/3} \qquad \text{for } \gamma = 7/5 \qquad \text{(A-7a)}$$

$$= \frac{W + 2}{24} \qquad \text{for } \gamma = 5/3 \qquad \text{(A-7b)}$$

$$\frac{\delta^*/\delta}{1 - W} \equiv D = 0.157 \qquad \text{for } \gamma = 7/5,\ W \geq 2 \qquad \text{(A-7c)}$$

$$= 0.176 \qquad \text{for } \gamma = 5/3,\ W \geq 2 \qquad \text{(A-7d)}$$

These expressions agree with the numerical integrations to within 3 percent.

Equations (A-7) have been used to evaluate K_o as a function of M_s, using the Sutherland viscosity relation for argon and for air. The results are given as Cases I and II in Table 2 in terms of β_o.

Real Gas

For strong shocks the previously noted ideal gas relations are no longer valid. The following procedure has therefore been used to obtain an estimate of the turbulent boundary layer behind a strong shock in air ($M_s \geq 6$).

The problem is to evaluate K_o (Eq. A-2) for a strong shock. First it was assumed that Eqs. (A-7a) and (A-7c) could be used with W obtained from the equilibrium shock solutions of Ref. 14. [Eqs. (A-7a) and (A-7c) agree with the limiting values of θ/δ and δ^*/δ obtained by strong shock assumptions, Eqs. (B-3), to within 5 percent and 8 percent for W = 10 and 15, respectively.] It then only remains to evaluate the term $[\quad]^{1/5}$ in Eq. (A-2). The energy equation for a strong shock gives

$$\frac{h_r}{h_{e,o}} = 1 + \frac{W - 1}{W + 1} r(0) \qquad \text{(A-8)}$$

with $r(0) = 0.897$ for air. Reference 14 was used to find W and $T_{e,o}/T_\infty = T_{e,o}/T_w$ for given M_s, p_∞, and $T_w = 300^\circ K$. It was then

assumed that $\rho_{e,o}/\rho_w \approx h_w/h_{e,o} \approx T_w/T_{e,o}$. The latter, with Eq. (A-8), permits $h_m/h_{e,o} \approx T_m/T_{e,o} \approx \rho_{e,o}/\rho_m$ to be found and Eq. (A-2) to be evaluated. The assumption that $h \approx T \approx 1/\rho$ is only approximately correct but should be sufficiently accurate for the present purposes (i.e., evaluation of $[\ ]^{1/5}$ in Eq. A-2).

The resulting values of K_o are also given in Table 2 (in terms of β_o). This table, together with Eq. (7), defines the turbulent boundary layer behind a strong shock in air. It should be kept in mind that the turbulent boundary layer theory of Refs. 11 and 12 has not been verified for strong shocks and that further simplifying assumptions were made to obtain K_o.

Boundary Layer Theory for Local Similarity Approximation

The turbulent boundary layer equations will be put in a form that is appropriate for an origin at ℓ_i, a wall velocity u_w, and free stream conditions u_e, ρ_e, which are isentropically related to conditions directly behind the shock ($u_{e,o}$, $\rho_{e,o}$). This boundary layer is illustrated in Fig. 3 and is used in the local similarity approximation in the body of the report.

For the boundary layer in Fig. 3, Eq. (A-1) becomes

$$-\delta^* = K\left(\frac{\nu_w}{u_w - u_e}\right)^{1/5} (\ell - \ell_i)^{4/5}$$

$$= K_o\left[\frac{K}{K_o}\left(\frac{\nu_w}{\nu_{w,o}}\frac{W-1}{W-V}\right)^{1/5}\right]\left(\frac{\nu_{w,o}}{u_w - u_{e,o}}\right)^{1/5} (\ell - \ell_i)^{4/5} \qquad \text{(A-9)}$$

where $V = u_e/u_{e,o}$. Equations (A-7) have the form

$$\frac{\theta/\delta}{1 - (W/V)} = \frac{B + (W/V)}{C} \qquad \text{(A-10a)}$$

$$\frac{\delta^*/\delta}{1 - (W/V)} = D \qquad \text{(A-10b)}$$

where B, C and D are constants. If the free stream Mach number relative to the shock, $M_{e,o} = (u_e/a_e)_o$, is small (i.e., strong shock), then the variation of fluid state properties in the free stream can be neglected ($\rho_e = \rho_{e,o}$; $p_e = p_{e,o}$), and Eqs. (A-9) and (A-10) then yield

$$\overline{\delta} = \frac{4V(-\delta^*)}{d} = H_e(\ell - \ell_i)^{4/5} \qquad \text{(A-11a)}$$

where

$$H_e = \frac{4K_o}{d}\left(\frac{W - V}{W - 1}\right)^{8/5}\left(\frac{W + B}{W + BV}\right)^{4/5}\left(\frac{\nu_{w,o}}{u_w - u_{e,o}}\right)^{1/5} \qquad \text{(A-11b)}$$

Note that B = 7/3 for air and 2 for argon (Eq. A-7).

APPENDIX B

Limiting Forms for θ/δ and δ^*/δ

Limiting forms for θ/δ and δ^*/δ are presented herein for the cases of both very weak shocks and very strong shocks.

Weak Shock

For the case of a weak shock, Eqs. (A-4) become

$$\frac{\delta^*/\delta}{1 - W} = \frac{\gamma}{8}[1 + 0(W - 1)] \qquad \text{(B-1a)}$$

$$\frac{\theta/\delta}{1 - W} = \frac{1}{8}[1 + 0(W - 1)] \qquad \text{(B-1b)}$$

Strong Shock

For strong shocks, $b \gg 1$, $c \gg 1$ and the ratio c/b has a limiting value given by

$$\frac{c}{b} = \frac{r(0)}{\gamma + r(0)} \qquad \text{Ideal Gas} \qquad \text{(B-2a)}$$

$$= \frac{r(0)}{[(W + 1)/(W - 1)] + r(0)} \qquad \text{Real Gas} \qquad \text{(B-2b)}$$

Thus $c/b = 0.391$, 0.344 for $\gamma = 1.4$, $r(0) = 0.897$ and $\gamma = 5/3$, $r(0) = 0.875$, respectively. These are the values for ideal air and argon. For a real gas with $r(0) = 0.9$, it follows that $c/b = 0.375$, 0.424, and 0.440 for $W = 5$, 10, and 15, respectively.

If terms of order b^{-1} compared with 1 are neglected, Eqs. (A-4) yield

$$\frac{\delta^*/\delta}{1 - W} = \frac{1}{W - 1}\left\{7\left(1 - \frac{c}{b}\right)\sum_{N=0}^{\infty}\frac{(c/b)^N}{7 + N}\left[\frac{W}{6 + N} + 1\right]\left[1 + 0(b^{-1})\right] - 1\right\}$$

$$\equiv D\left(\frac{W - E}{W - 1}\right)\left[1 + 0(b^{-1})\right] \qquad \text{(B-3a)}$$

$$\frac{\theta/\delta}{1 - W} = 7\left(1 - \frac{c}{b}\right)\sum_{N=0}^{\infty}\frac{(c/b)^N}{(7 + N)(8 + N)}\left(\frac{2W}{6 + N} + 1\right)\left[1 + 0(b^{-1})\right]$$

$$\equiv \frac{W + B}{C}\left[1 + 0(b^{-1})\right] \qquad \text{(B-3b)}$$

The constants, B, C, D, E have been evaluated for several values of c/b and are given in Table 4.

For strong shocks in air, Eqs. (A-7a) and (A-7c) agree with Eqs. (B-3) to within 5 percent for W = 10 and to within 8 percent for W = 15. Hence Eqs. (A-7a) and (A-7c) are sufficiently accurate for a first estimate of θ and δ^* behind strong shocks in air.

Table 4. Constants Defining θ/δ and δ^*/δ for Strong Shocks (Eqs. B-3)

c/b	B	C	D	D
0.35	3.16	28.2	0.148	0.413
0.40	3.19	29.2	0.144	0.511
0.45	3.23	30.3	0.140	0.632
0.50	3.27	31.6	0.135	0.781

REFERENCES

1. R. E. Duff, "Shock-Tube Performance at Low Initial Pressure," Phys. Fluids 2 (2), 207-16 (1959).

2. A. Roshko, "On Flow Duration in Low-Pressure Shock Tubes," Phys. Fluids 3 (6), 835-42 (1960).

3. W. J. Hooker, "Testing Time and Contact-Zone Phenomena in Shock Tube Flows," Phys. Fluids 4 (12), 1451-63 (1961).

4. H. Mirels, "Test Time in Low Pressure Shock Tubes," TDR-169(3230-12)TN-5, Aerospace Corporation, El Segundo, Calif. (27 December 1962).

5. G. F. Anderson, "Shock-Tube Testing Time," J. Aero/Space Sci. 26 (3), 184-5 (1959).

6. P. H. Rose and W. I. Stark, "Stagnation Point Heat-Transfer Measurements in Dissociated Air," J. Aeronaut. Sci. 25 (2), 86-97 (1958).

7. R. A. Hartunian, A. L. Russo, and P. V. Marrone, "Boundary-Layer Transition and Heat Transfer in Shock Tubes," J. Aerospace Sci. 27 (8), 587-94 (1960).

8. J. Gordon Hall, "Shock Tubes. Part II: Production of Strong Shock Waves; Shock Tube Applications, Design, and Instrumentation," UTIA Review No. 12 (May 1958).

9. C. E. Wittliff and M. R. Wilson, "Shock Tube Driver Techniques and Attenuation Measurements," Cornell Aeronautical Lab. Rept. No. AD-1052-A-4. (August 1957).

10. J. J. Jones, "Experimental Investigation of Attenuation of Strong Shock Waves in a Shock Tube with Hydrogen and Helium as Driver Gases," NACA TN 4072 (July 1957).

11. H. Mirels, "Boundary Layer Behind Shock or Thin Expansion Wave Moving into Stationary Fluid," NACA TN 3712 (1956).

12. H. Mirels, "The Wall Boundary Layer Behind a Moving Shock Wave," Boundary Layer Research, Proc. International Union of Theoretical and Applied Mechanics, ed. H. Gortler (Springer Verlag, Berlin, 1958), pp. 283-293.

13. W. A. Martin "An Experimental Study of the Turbulent Boundary Layer Behind the Initial Shock Wave in a Shock Tube," J. Aero/Space Sci. 25 (10), 644-52 (1958).

14. S. Feldman, "Hypersonic Gas Dynamic Charts for Equilibrium Air," AVCO Research Report No. 40 (1957).

15. H. Mirels, "Attenuation in a Shock Tube Due to Unsteady-Boundary Layer Action." NACA Report 1333 (1957). (Supersedes NACA TN 3278).

16. H. Mirels and W. H. Braun, "Nonuniformities in Shock Tube Flow Due to Unsteady Boundary Layer Action," NACA TN 4021 (1957).

Aerospace Corporation, El Segundo, California. SHOCK TUBE TEST TIME LIMITATION DUE TO TURBULENT WALL BOUNDARY LAYER, prepared by Harold Mirels. 6 May 1963. [62] p. incl. illus. (Report TDR-169(3230-12)TR-3; SSD-TDR-63-78) (Contract AF 04(695)-169) Unclassified report

Shock tube test time limitation due to the premature arrival of the contact surface is analytically investigated for wholly turbulent wall boundary layers. The results are compared with those for wholly laminar wall boundary layers. It is found that for a given shock Mach number, M_s, the maximum possible test time (in a long shock tube) varies as $d^{5/4}p_\infty^{1/4}$ and d^2p_∞ for the turbulent and laminar cases, respectively (d = tube diam, p_∞ = initial pressure). For $3 \leq M_s \leq 8$ in air or argon, it is found that the turbulent boundary layer theory for maximum test time applies for $dp_\infty \gtrsim 4$ to 10 (air) and $dp_\infty \gtrsim 2$ to 10 (argon), where d is in

(over)

UNCLASSIFIED

UNCLASSIFIED

Aerospace Corporation, El Segundo, California. SHOCK TUBE TEST TIME LIMITATION DUE TO TURBULENT WALL BOUNDARY LAYER, prepared by Harold Mirels. 6 May 1963. [62] p. incl. illus. (Report TDR-169(3230-12)TR-3; SSD-TDR-63-78) (Contract AF 04(695)-169) Unclassified report

Shock tube test time limitation due to the premature arrival of the contact surface is analytically investigated for wholly turbulent wall boundary layers. The results are compared with those for wholly laminar wall boundary layers. It is found that for a given shock Mach number, M_s, the maximum possible test time (in a long shock tube) varies as $d^{5/4}p_\infty^{1/4}$ and d^2p_∞ for the turbulent and laminar cases, respectively (d = tube diam, p_∞ = initial pressure). For $3 \leq M_s \leq 8$ in air or argon, it is found that the turbulent boundary layer theory for maximum test time applies for $dp_\infty \gtrsim 4$ to 10 (air) and $dp_\infty \gtrsim 2$ to 10 (argon), where d is in

(over)

UNCLASSIFIED

UNCLASSIFIED

Aerospace Corporation, El Segundo, California. SHOCK TUBE TEST TIME LIMITATION DUE TO TURBULENT WALL BOUNDARY LAYER, prepared by Harold Mirels. 6 May 1963. [62] p. incl. illus. (Report TDR-169(3230-12)TR-3; SSD-TDR-63-78) (Contract AF 04(695)-169) Unclassified report

Shock tube test time limitation due to the premature arrival of the contact surface is analytically investigated for wholly turbulent wall boundary layers. The results are compared with those for wholly laminar wall boundary layers. It is found that for a given shock Mach number, M_s, the maximum possible test time (in a long shock tube) varies as $d^{5/4}p_\infty^{1/4}$ and d^2p_∞ for the turbulent and laminar cases, respectively (d = tube diam, p_∞ = initial pressure). For $3 \leq M_s \leq 8$ in air or argon, it is found that the turbulent boundary layer theory for maximum test time applies for $dp_\infty \gtrsim 4$ to 10 (air) and $dp_\infty \gtrsim 2$ to 10 (argon), where d is in

UNCLASSIFIED

UNCLASSIFIED

Aerospace Corporation, El Segundo, California. SHOCK TUBE TEST TIME LIMITATION DUE TO TURBULENT WALL BOUNDARY LAYER, prepared by Harold Mirels. 6 May 1963. [62] p. incl. illus. (Report TDR-169(3230-12)TR-3; SSD-TDR-63-78) (Contract AF 04(695)-169) Unclassified report

Shock tube test time limitation due to the premature arrival of the contact surface is analytically investigated for wholly turbulent wall boundary layers. The results are compared with those for wholly laminar wall boundary layers. It is found that for a given shock Mach number, M_s, the maximum possible test time (in a long shock tube) varies as $d^{5/4}p_\infty^{1/4}$ and d^2p_∞ for the turbulent and laminar cases, respectively (d = tube diam, p_∞ = initial pressure). For $3 \leq M_s \leq 8$ in air or argon, it is found that the turbulent boundary layer theory for maximum test time applies for $dp_\infty \gtrsim 4$ to 10 (air) and $dp_\infty \gtrsim 2$ to 10 (argon), where d is in

UNCLASSIFIED

inches, p_{∞} is in cm Hg. Similarly, for $3 \leq M_s \leq 8$, the laminar theory applies for $dp_{\infty} \lesssim 0.3$ (air) and $dp_{\infty} \lesssim 0.6$ to 1 (argon). When $dp_{\infty} \approx 5$, turbulent theory for both air and argon indicates test times of about 1/2 to 1/4 the ideal value for $x_s/d = 45$ to 150, respectively (x_s = length of low pressure section). Higher values of dp_{∞} result in more test time. When $dp_{\infty} \approx 0.5$, laminar theory indicates about 1/2 ideal test time for $x_s/d \approx 100$. Lower dp_{∞} reduces test time. Working curves are presented for more accurate estimates of test time in specific cases.

UNCLASSIFIED

UNCLASSIFIED

inches, p_{∞} is in cm Hg. Similarly, for $3 \leq M_s \leq 8$, the laminar theory applies for $dp_{\infty} \lesssim 0.3$ (air) and $dp_{\infty} \lesssim 0.6$ to 1 (argon). When $dp_{\infty} \approx 5$, turbulent theory for both air and argon indicates test times of about 1/2 to 1/4 the ideal value for $x_s/d = 45$ to 150, respectively (x_s = length of low pressure section). Higher values of dp_{∞} result in more test time. When $dp_{\infty} \approx 0.5$, laminar theory indicates about 1/2 ideal test time for $x_s/d \approx 100$. Lower dp_{∞} reduces test time. Working curves are presented for more accurate estimates of test time in specific cases.

UNCLASSIFIED

UNCLASSIFIED

inches, p_{∞} is in cm Hg. Similarly, for $3 \leq M_s \leq 8$, the laminar theory applies for $dp_{\infty} \lesssim 0.3$ (air) and $dp_{\infty} \lesssim 0.6$ to 1 (argon). When $dp_{\infty} \approx 5$, turbulent theory for both air and argon indicates test times of about 1/2 to 1/4 the ideal value for $x_s/d = 45$ to 150, respectively (x_s = length of low pressure section). Higher values of dp_{∞} result in more test time. When $dp_{\infty} \approx 0.5$, laminar theory indicates about 1/2 ideal test time for $x_s/d \approx 100$. Lower dp_{∞} reduces test time. Working curves are presented for more accurate estimates of test time in specific cases.

UNCLASSIFIED

UNCLASSIFIED

inches, p_{∞} is in cm Hg. Similarly, for $3 \leq M_s \leq 8$, the laminar theory applies for $dp_{\infty} < 0.3$ (air) and $dp_{\infty} < 0.6$ to 1 (argon). When $dp_{\infty} \approx 5$, turbulent theory for both air and argon indicates test times of about 1/2 to 1/4 the ideal value for $x_s/d = 45$ to 150, respectively (x_s = length of low pressure section). Higher values of dp_{∞} result in more test time. When $dp_{\infty} \approx 0.5$, laminar theory indicates about 1/2 ideal test time for $x_s/d \approx 100$. Lower dp_{∞} reduces test time. Working curves are presented for more accurate estimates of test time in specific cases.

UNCLASSIFIED